Residues Neighboring an SH3-Binding Motif Participate in Determining Affinity and Specificity *In Vivo*

David F. Jordan[1,2,3,4,*], Alexandre K. Dubé[1,2,3,4,5], Ugo Dionne[2,3,4,6,7,8], David Bradley[1,2,3,4,5] and Christian R. Landry [1,2,3,4,5,*]

1. Département de Biochimie, microbiologie et bio-informatique, Université Laval, 1045 Avenue de la Médecine,Québec, QC, Canada, G1V 0A6
2. Institut de Biologie Intégrative et des Systèmes (IBIS), 1030, Avenue de la Médecine, Université Laval, Québec, QC, Canada, G1V 0A6
3. PROTEO-Regroupement Québécois de Recherche sur la Fonction, l'Ingénierie et les Applications des Protéines, Université Laval, 1030, Avenue de la Médecine Québec, QC, Canada, G1V 0A6
4. Centre de Recherche en Données Massives de l'Université Laval, Université Laval, 1065, Avenue de la Médecine, Québec, QC, Canada, G1V 0A6
5. Département de Biologie, Université Laval, 1045 Avenue de la Médecine, Québec, QC, Canada, G1V 0A6
6. Centre de Recherche du Centre Hospitalier Universitaire (CHU) de Québec-Université Laval, 11, côte du Palais, Québec, QC, Canada, G1R 2J6
7. Centre de Recherche sur le Cancer de l'Université Laval, 9, rue McMahon, Québec, QC, Canada, G1R 3S3
8. Present address: Lunenfeld-Tanenbaum Research Institute, Sinai Health, 600 University Avenue, Toronto, ON, Canada, M5G 1X5

* Correspondence: 1030, Avenue de la Médecine, Université Laval, Québec, QC, Canada, G1V 0A6 Email: david.jordan.2@ulaval.ca. 1030, Avenue de la Médecine, Université Laval, Québec, QC, Canada, G1V 0A6 Email: christian.landry@bio.ulaval.ca

Running head: Determining affinity and specificity *in vivo*

Keywords: Binding motif, Src Homology 3 (SH3) domain, Deep mutational scanning, Binding affinity, Binding specificity, Structure prediction

Abstract

In signaling networks, many protein-protein interactions are mediated by modular domains that bind short linear motifs. The motifs' sequences modulate many factors, among them affinity and specificity, or the ability to bind strongly and to bind the appropriate partners. Previous studies have proposed a trade-off between affinity and specificity, suggesting that motifs with high affinity are less capable of differentiating between domains with similar sequences and structures. Using Deep Mutational Scanning to create a mutant library of a well characterized binding motif, and protein complementation assays to measure protein-protein interactions, we tested this trade-off *in vivo* for the first time. We measured the binding strength and specificity of a library of mutants of a binding motif on the MAP kinase kinase Pbs2, which binds the SH3 domain of the osmosensor protein Sho1 in *Saccharomyces cerevisiae*. We find that many mutations in the region surrounding the binding motif modulate binding strength, but that few mutations have a strong impact on specificity. Moreover, we find no systematic relationship between affinity and specificity as measured *in vivo*. Interestingly, all Pbs2 mutations which increase affinity or specificity are situated outside of the Pbs2 residues that interact with the canonical SH3-binding pocket, suggesting that other surfaces on Sho1 contribute to binding. We use predicted structures to propose a model of binding which involves residues neighboring the core Pbs2 motif binding outside of the canonical SH3-binding pocket, allowing affinity and specificity to be determined by a broader range of sequences than what has previously been considered.

Summary

Protein-protein interactions are often mediated by a binding domain on one protein and a short disordered binding motif on another protein. We measured the binding strength and specificity of a mutant library of a binding motif situated in the yeast protein Pbs2. We find no trade-off between the two factors, contrary to what has previously been suggested. We also use protein structure prediction to propose that interactions take place between residues outside of the canonical motif and binding pocket.

Introduction

Cells possess complex and robust signaling networks that detect stimuli and trigger responses. These signaling networks are composed of a series of protein-protein interactions, which are often mediated by modular interaction domains. Many classes of protein interaction domains involved in signaling are shared across pathways and species, yet fill different roles and functions (Pawson *et al.* 2002). The different constraints placed on interaction domains by their distinct roles contribute to explaining the divergence in sequence between homologs of the same domain (Ernst *et al.* 2010; Dionne *et al.* 2022). Therefore, to understand how domain sequences have evolved and continue to evolve, the phenotypic consequences of mutations must be understood. Two of the major phenotypes for protein-protein interaction domains are affinity, that is, the strength of binding to the partner protein, and specificity, that is, the ability to bind to the appropriate partner proteins, and to not form spurious interactions with other proteins in the cellular environment (Ivarsson and Jemth 2019).

Many interaction domains bind short intrinsically disordered stretches of their interaction partners, also known as short linear motifs (SLiMs) or simply binding motifs (Gouw *et al.* 2018). Interactions mediated by domain-motif associations are relatively weak, with dissociation constants (K_D) in the micromolar range, while domain-domain binding typically results in dissociation constant values orders of magnitude smaller, indicating much stronger binding (Van Roey *et al.* 2014). While such low affinity could be caused by physical limitations, such as the smaller interface, other hypotheses have been put forward which suggest that an overly strong affinity can have deleterious effects on the cell, for instance by compromising specificity (Haslam and Shields 2012; Karlsson *et al.* 2016). In fact, protein binding domains, and reciprocally binding motifs, are under positive or purifying selection for binding with peptide sequences for which interactions lead to beneficial outcome. At the same time, they are under selection against interactions that negatively impact cells growth and survival. In particular, binding proteins are thought to be under selection to not spuriously bind proteins in the cellular network other than their appropriate binding partners (Zarrinpar *et al.* 2003). The balance between selection for binding with partners and selection against spurious binding could shape the binding domain or motif to bind specifically rather than strongly. This dual selection likely acts across molecular networks, and in the long term could have led to the evolution of the canonical signaling pathways that we find in extant species. However, the extent to which existing systems represent a compromise between affinity and specificity depends on the assumption that the two phenotypes cannot be optimized independently. Certain mutations could affect only one of the two phenotypes, or other components of proteins could play a part in shaping these phenotypes. To test for such an affinity-specificity trade-off, these two phenotypes would have to be measured for a large number of mutations, ideally in their cellular context, as many extrinsic factors can contribute to specificity and affinity, apart from domain and motif sequences.

Binding affinity and specificity have previously been explored in the context of the interaction between binding domains and motifs, by measuring the binding of mutants *in vitro* (Zarrinpar *et al.* 2003; Vincentelli *et al.* 2015; Kazlauskas *et al.* 2016). However, the interaction of proteins in the cellular environment is a more complex situation, and many interactions detected *in vivo* are

not detected *in vitro* (Kelil *et al.* 2017). Many factors can modulate binding in the cell, including colocalization of partners, expression in the same cell cycle phases, and contributions from sequences outside of the immediate binding domain and motif, as well as other proteins that can interact with one or both of the partners (Ivarsson and Jemth 2019; Dionne *et al.* 2022). More recently, studies have begun to use techniques such as deep mutational scanning (DMS) to study the impact of large libraries of mutations on protein stability and function *in vivo* (Fowler and Fields 2014). Methods such as protein complementation assays (Tarassov *et al.* 2008; Michnick *et al.* 2016) have also successfully been used to measure the *in vivo* binding strength of libraries of mutants in yeast (Diss and Lehner 2018; Dionne *et al.* 2021; Faure *et al.* 2022; Robles *et al.* 2023; Bendel *et al.* 2023; Dibyachintan *et al.* 2024). For example, a recent study showed the effect on binding of combining mutations in a PDZ domain and its binding motif (Zarin and Lehner 2024). These *in vivo* techniques could be used to determine how mutations can affect domain-motif interaction affinity and specificity.

One powerful model to study domain-motif interactions are SH3 domains. These globular domains are composed of around 60 residues, and bind different classes of polyproline motifs defined by the canonical forms R/KXXPXXP for class I and PXXPXR/K for class II (Kaneko *et al.* 2008). The model yeast *Saccharomyces cerevisiae* contains 27 different SH3 domains (Dionne *et al.* 2022), including one in the High Osmolarity Glycerol (HOG) signaling pathway protein Sho1 (Saito and Posas 2012). The SH3 domain of Sho1 is known to interact with a motif on the MAPKK Pbs2, and this binding can be substantially strengthened by exposing cells to osmotic stress (Maeda *et al.* 1995; Posas and Saito 1997; Saito and Posas 2012) (Figure 1a). The Sho1-Pbs2 domain-motif interaction is thus a powerful model to study domain-motif interaction strength and specificity, due to Pbs2's potential for off-target interactions and the simple method of inducing an increase in the interaction strength.

To better understand the impact of mutations on affinity and specificity, we measured the binding properties of a nearly complete library of mutations in the Pbs2 binding motif *in vivo* using a DHFR Protein-fragment Complementation Assay (PCA) (Tarassov *et al.* 2008; Michnick *et al.* 2016). We measured the binding strength between single residue Pbs2 motif mutants and Sho1, the canonical partner of Pbs2. We also measured the off-target interactions of selected Pbs2 binding motif mutants with SH3 domain containing proteins other than Sho1. We show that mutations in Pbs2 can affect both interaction strength with Sho1 and other SH3 containing proteins in the cell, although very few single mutations are able to substantially modify the specificity of Pbs2 for Sho1. We also find that all single mutations that increase the interaction strength and specificity are found outside the canonical binding motif, and that certain residues outside the binding motif are predicted to interact with Sho1 outside of the canonical binding pocket, and even outside of the SH3 domain.

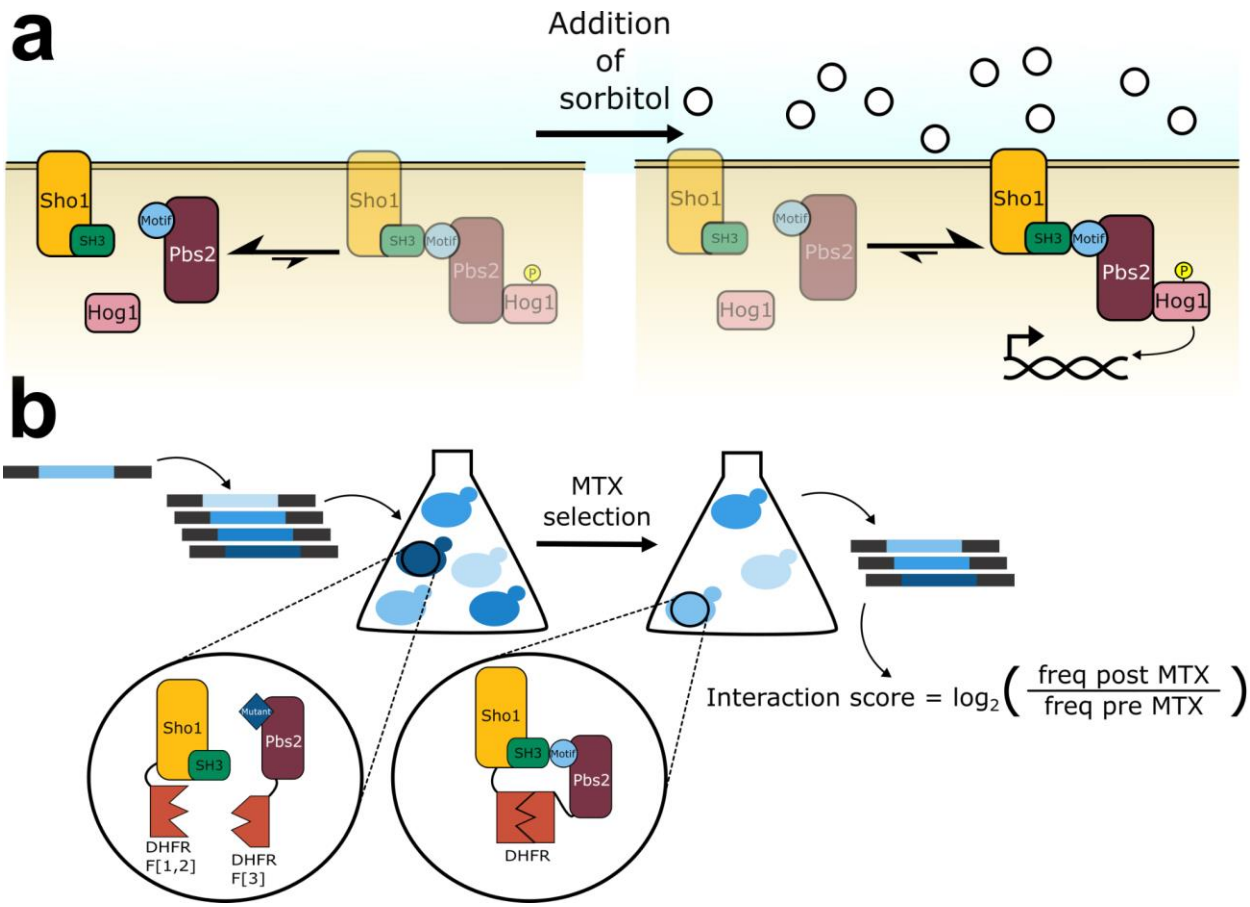

Figure 1. The Sho1-Pbs2 interaction can be strengthened using sorbitol exposure, and the DHFR-PCA can be used to measure the interaction strength between Sho1 and Pbs2.
a) Simplified schematic of the HOG pathway, and the interactions between Sho1, Pbs2 and Hog1. In normal conditions (left), Sho1, Pbs2 and Hog1 are mostly separated. In the presence of osmotic stress such as sorbitol (right), the signaling through the pathway is induced, the proteins assemble into a complex, and Hog1 is phosphorylated, which causes it to modulate gene expression via translocation to the nucleus. b) Schematic of the DHFR-PCA screen with a DMS mutant library. Single residue variants of *PBS2* were inserted into the yeast genome at the natural locus using CRISPR-Cas9 genome editing. Sho1 and Pbs2 were tagged with complementary fragments of the murine DHFR. In cases where the Pbs2 variant does not interact with Sho1, the DHFR fragments remain separated. Upon interaction between a Pbs2 variant and Sho1, the DHFR fragments combine to reconstitute the functional murine DHFR, and allow growth in the presence of methotrexate (MTX). More strongly interacting partners allow the cell to proliferate more rapidly. The interaction score is calculated as the log2-fold change in variant frequency before and after the selection by MTX (Freschi *et al.* 2013).

Results

Scan of the region surrounding the Pbs2 motif reveals that few mutations modify binding to Sho1

The interaction between Sho1 and Pbs2 is modulated by an SH3 domain on Sho1 and the binding motif on Pbs2, which is a type I motif with the sequence KPLPPLP (Maeda *et al.* 1995). Previous computational work has suggested that the region surrounding binding motifs could play an important role in modulating binding, including in SH3 interactions and in particular in the Sho1-Pbs2 interaction (Stein and Aloy 2008; Kelil *et al.* 2016). To determine which Pbs2 residues play a role in binding, we undertook a Deep Mutational Scan (DMS) on a region of 56 codons comprising the binding motif and its surrounding region. A DNA library of every possible single codon mutant was created for the 56 codon stretch, and inserted into the *S. cerevisiae* genome at the PBS2 locus using a CRISPR Cas-9 based approach, replacing the wild-type sequence (Dionne *et al.* 2021). This was done in a strain with a Dihydrofolate Reductase Protein-Fragment 3 (DHFR F[3]) fusion at the C-terminus of *PBS2*. This mutant library of yeast cells was mated with Sho1-DHFR F[1,2] cells, in order to obtain diploid strains containing complementary DHFR F fusions on both interaction partners. In a Dihydrofolate Reductase - Protein-Fragment Complementation Assay (DHFR-PCA), an interaction between the tagged proteins brings the two DHFR fragments into contact, forming a functional murine DHFR which allows cell division even in the presence of methotrexate (MTX), an inhibitor of the endogenous yeast DHFR (Figure 1b). Growth in the presence of MTX in a strain with both DHFR fragments is therefore a proxy for the amount of Sho1-Pbs2 complexes forming, which depends on both the binding affinity and the local abundance of the interacting proteins (Tarassov *et al.* 2008; Freschi *et al.* 2013).

To measure the interaction strength of the DMS library, the mutants were pooled and DHFR-PCA competition assays were done in media containing both MTX and 1 M of sorbitol, in order to induce the HOG pathway (Ferrigno *et al.* 1998). The resulting interaction score was calculated as the log-2-fold change of variant frequencies before and after selection for the interaction using MTX, as detected by targeted sequencing of the *PBS2* locus. Variants that increase protein complex formation and therefore allow more growth in the presence of MTX rise in frequency, and have a positive interaction score. Variants with reduced amounts of complex formation are depleted during the DHFR-PCA, and have negative interaction scores.

We found that most mutations in the region surrounding the motif did not affect binding of Sho1, apart from a short section adjacent to the motif itself in positions 93 to 99 (Figure 2a, Figure S1, Figure S2a). This confirms the strong role of the motif in the interaction and validates the computational predictions that extended the role of binding to include neighboring residues (Stein and Aloy 2008; Kelil *et al.* 2016). Since the effect on binding was strongly position dependent, we categorized different sections of Pbs2 as follows: the core motif is the conserved type I binding motif sequence situated in positions 93 to 99, the extended motif is composed of the core motif and the neighboring residues which have a strong impact on binding from positions 85 to 100, the flanking sequences are the remaining positions in the DMS library, namely positions 71 to 84 and 101 to 126 (Figure 2b).

As mentioned above, DHFR-PCA reports on the amount of protein complex formed, which depends on affinity and local protein abundance. To differentiate between these two parameters, we measured the effect of mutations on Pbs2 binding to a partner that does not depend on the SH3 binding motif. Hog1 is a transcriptional activator that binds distally to the SH3 binding motif of Pbs2 (Murakami *et al.* 2008) (Figure 1a). Hog1 binding to Pbs2 is independent of Sho1 binding and the Sho1 binding motif (Murakami *et al.* 2008), and so measuring Pbs2-Hog1 binding through DHFR-PCA controls for Pbs2 local abundance. Pbs2 motif mutations that reduce growth during the DHFR-PCA assay by affecting Sho1 binding should have no effect on the Pbs2-Hog1 DHFR-PCA, while motif mutations that reduce DHFR complementation through destabilization of Pbs2 or reduction of local Pbs2 abundance should have a negative impact on the Pbs2-Sho1 interaction as well as the Pbs2-Hog1 interaction. Mutations that increase the abundance of Pbs2 can also be detected, as they should lead to higher Hog1-Pbs2 interaction scores. As the DHFR fusions are at the C-terminus, nonsense mutations introduced in the mutant library lead to no DHFR fragment expression. Nonsense mutants therefore represent an absence of reconstituted DHFR complexes, and no signal in the DHFR-PCA.

We found that most mutations in the surrounding region of the Pbs2 motif had little effect on Hog1 binding (Figure 2a). Furthermore, mutants that had a negative effect on Hog1-Pbs2 binding also had a negative effect on Sho1-Pbs2 binding, suggesting that the reduction in signal results from a loss of local abundance of Pbs2 (Figure S3). However, most mutations affected Sho1 binding without impacting the Hog1 interaction, and therefore without affecting the local abundance of Pbs2. In particular, some mutations reduce the Sho1-Pbs2 interaction below the detectable level, which represents as little growth as nonsense mutations. Strikingly, only mutations in the residues comprising the extended motif had Sho1-interaction specific effects, while mutations in the flanking sequences of the motif had either little effect or destabilizing effects.

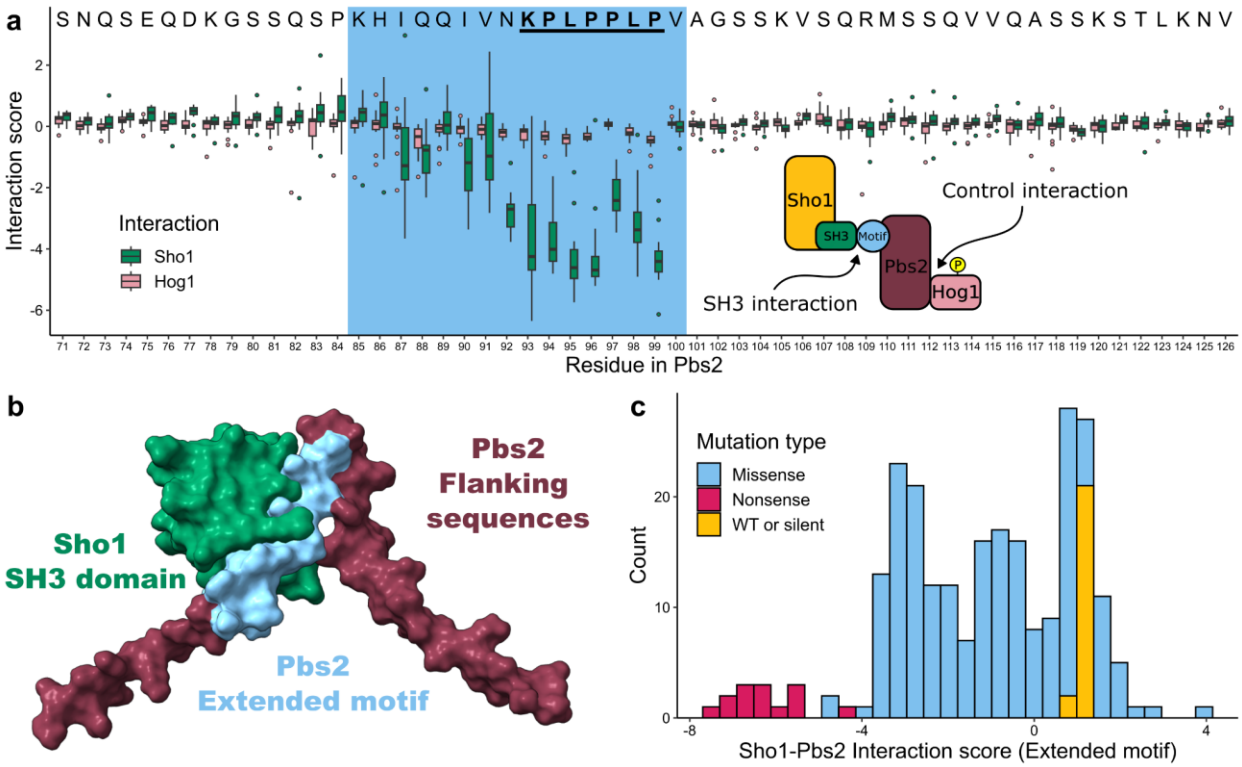

Figure 2. Mutations in Pbs2 within and around the binding motif affect binding to Sho1. a) Effect of Pbs2 mutations in the surrounding region of the SH3 binding motif (interaction score, log2-fold change before and after selection using MTX), with either Sho1 or Hog1. The wild-type residues of Pbs2 are indicated for each position at the top of the figure. The positions comprising the extended motif are highlighted in blue, while the positions in the core motif have the wild-type residue indicated in bold and underlined. b) A predicted structure (AlphaFold2-Multimer) of the SH3 domain of Sho1 (green) in complex with the Pbs2 region surrounding the motif. The Pbs2 surrounding region is colored to identify the extended motif (light blue) and the flanking sequences (burgundy). c) Distribution of interaction scores between Sho1 and Pbs2 single mutants in the extended motif DMS library (positions 85 to 100). Mutations are colored by the nature of the mutation, either a change to a stop codon (nonsense), a change to the wild-type codon or a synonymous codon (WT or silent) or a change to a codon coding for a different residue (missense).

Extended motif DMS library identifies mutations modulating interaction strength

In light of these results, we decided to focus solely on the extended motif of Pbs2 comprising codons 85 to 100. In our first DMS library, due to the mating of the DHFR F[1,2] strain and the DHFR F[3] strain resulting in a diploid strain, a large part of Pbs2 binding was with the copy of Sho1 which was originally from the DHFR F[3] strain, and which had no DHFR F[1,2] tag. Consequently these interactions did not contribute to growth in the presence of methotrexate. This limited our ability to precisely measure the Sho1-Pbs2 interaction. We therefore constructed

two haploid strains with two DHFR fragments, with DHFR F[3] on Pbs2 and DHFR F[1,2] on Sho1 in the first strain and on Hog1 in the second. We constructed a second DMS library for only the extended motif, containing all possible NNK codons (all codons with a G or T in the 3' position). This library was inserted into the haploid DHFR F[1,2]/DHFR F[3] strains using the same CRISPR-Cas9 based approach as with the previous assay. Once more, this allowed the measurement of binding strength to Sho1 as a proxy for affinity and binding strength to Hog1 as a proxy of local abundance and protein stability, but this time without the interference of a non-tagged copy of Sho1 or Hog1. The interaction strength of the variants was measured using the DHFR-PCA as previously (Figure S1b, Figure S4). At this point, we filtered out the 23 mutants which had an interaction score with Hog1 significantly different from wild type and synonymous Pbs2 mutants (Mann-Whitney U test with false discovery rate corrected p-value < 0.05) from our analysis (Figure S5). As before, the goal was to disregard mutants which modulated the interaction through change of local abundance or stability, which would affect both the Sho1 and Hog1 interaction.

The impacts on the Sho1-Pbs2 interaction were varied (Figure 2c, Figure S6). Few mutants had interaction scores as low as the nonsense mutants, suggesting that few single mutations are able to completely prevent Sho1-Pbs2 binding. By comparing mutant interaction scores to the wild type and synonymous mutants scores, we found that many mutants had significantly (Mann-Whitney U test with false discovery rate corrected p-value <= 0.05) stronger or weaker scores than the wild-type Pbs2 sequence. 25 mutants (9.3% of all mutants) interacted significantly more strongly with Sho1 than wild-type Pbs2, while 178 mutants (66.2% of all mutants) interacted significantly more weakly than wild-type Pbs2. The impact of mutants that reduced the interaction scores was generally greater.

As the Sho1-Pbs2 interaction is strengthened under osmotic stress (Maeda *et al.* 1995; Posas and Saito 1997; Saito and Posas 2012), we also compared the interaction strength between these two proteins in the presence and absence of 1 M of sorbitol (Figure S7). We found that interaction scores in the presence and absence of sorbitol correlate strongly (Spearman's rho 0.98, p-value $< 2.2X10^{-16}$). The effects on binding were stronger in the presence of sorbitol, as a result of the induction of the HOG signaling pathway. WHen sorbitol is present, strongly interacting Pbs2 mutants are even more often in contact with Sho1, increasing the number of reconstituted DHFR complexes, while weakly interacting mutants are even further outcompeted by the strongly interacting mutants. Still, the high correlation in interaction scores between these two conditions indicates that Pbs2 mutants behave similarly in the presence and absence of osmotic stress, and that the general effect of mutations does not depend on the activation of the signaling pathway.

To validate the pooled measurements, we individually reconstructed 24 mutants spanning the range of measured interaction scores in Pbs2-DHFR F[3] strains which were mated with a Sho1-DHFR F[1,2] strain. We then measured the growth rate of these mated strains in growth curves in DHFR-PCA medium. As with the competition assay, the growth rate is a proxy for interaction strength, which reflects affinity in the absence of a change in abundance. The growth curve results correlate strongly with the interaction scores (Spearman's rho 0.98, p-value $2.1x10^{-6}$ for interactions in presence of 1 M sorbitol, spearman's rho of 0.74, p-value $3.3x10^{-5}$ for interactions in absence of sorbitol), thus upholding the results of the competition assay (Figure S8a). To

confirm even further that the effects on interaction strength were not the result of noise or the result of another source, we also performed a smaller scale competition assay DHFR-PCA, individually reconstructing 67 mutants with varying interaction scores (Figure S2c). The measurements of this validation assay correlated strongly with the assay on the DMS library of the extended motif (Spearman's rho 0.97, $p < 2.2X10^{-16}$ for interactions in presence of 1 M sorbitol, spearman's rho of 0.96, $p < 2.2X10^{-16}$ for interactions in absence of sorbitol), thus confirming the results of the measurement of the DMS library Figure S8b). We also measured the effect of mutations on cell proliferation by constructing strains with the same 67 mutations, but with no DHFR tags. Cell growth and division should thus only depend on the effect of the mutations, and not interaction strength. We undertook a pooled competitive growth assay in SC synthetic media with 1 M of sorbitol, measuring how much each mutant proliferated. We found that all mutations except nonsense mutations had no significant effect on cell proliferation (Welch's t-test false discovery rate corrected p-value < 0.05) (Figure S9). Interestingly, mutant I87W, which is the strongest interacting mutation, seems to have a detectable, though not statistically significant, deleterious effect on cell proliferation.

<u>Few mutations change the binding strength of Pbs2 to SH3 containing proteins other than Sho1</u>

While Pbs2 is not known to bind to proteins other than Sho1 through its Sho1-binding motif, replacing the SH3 domain of Abp1 with the Sho1 SH3 domain leads to Pbs2 interacting with Abp1 (Dionne *et al.* 2021). This shows that if an SH3 domain capable of binding the Pbs2 Sho1-binding motif is present in another protein, this other protein can interact with Pbs2. Similarly, changes to the sequence of the Pbs2 motif could also lead to a better matching motif for other SH3 domains, leading to non-specific interactions. Accordingly, we verified if mutations in the core motif of Pbs2, in the extended motif, or in the surrounding region could modify binding specificity. Here we define loss of specificity as an increase of Pbs2 binding to SH3 domain containing proteins other than Sho1. Alternatively, a mutant could undergo a gain in specificity if it binds less strongly to other SH3 domain containing proteins. In other words, a loss of specificity is a gain of off-target interactions, and vice versa. One way to test this is to measure the binding of a Pbs2 mutant to a certain SH3 domain containing protein, and compare this interaction score to the interaction score of wild-type Pbs2 with the same protein (Figure 3a).

Following this reasoning, we measured the interaction strength of 32 chosen Pbs2 variants, including wild-type Pbs2 with the 24 SH3 containing proteins in yeast. We once again used the DHFR-PCA approach, adding DHFR F[3] tags to the Pbs2 variants and DHFR F[1,2] tags to the SH3 domain containing proteins. Pbs2 mutants with Sho1 interaction strengths spanning the range of possible affinities were selected, including a number of the strongest interacting mutants such as I87W, V91L, Q89D, H86W and V91C. The DHFR-PCA was conducted on solid media instead of in a pooled liquid competition assay, in order to measure individual combinations of Pbs2 mutants and SH3 containing proteins in individual colonies. Colonies containing all possible crosses were grown on solid DHFR-PCA media with 1 M sorbitol, which has the same effect as the liquid DHFR-PCA media of allowing growth proportional to the number of Sho1-Pbs2 complexes formed. Consequently, the colony sizes were used as a measurement interaction

strength. For this analysis, binding to Nbp2 was not considered, as Pbs2 is known to bind the SH3 domain of Nbp2 through a second, distal binding motif (Mapes and Ota 2004), and so an interaction was detected regardless of the mutation to the Sho1 binding motif.

Only three Pbs2 mutants (Q82W, P97A and L98F) were found to interact with an SH3 containing protein more strongly than wild-type Pbs2 with the same protein, indicating a loss of specificity, while six Pbs2 mutants interacted with an SH3 containing protein more weakly than wild-type Pbs2 (Q82W, S83F, K85W, I87W, N92H and N92S), indicating a gain in specificity (Welch's t-test with false discovery rate corrected p-value < 0.05) (Figure 3b, Figure S10). Interestingly, mutant Q82W displayed both loss and gain of specificity with different SH3 containing proteins, suggesting a more general shift in the interaction profile rather than a simple loss or gain of specificity. The SH3 domains involved in losses or gains of specificity possess divergent binding profiles, and bind motifs of different classes (Tonikian *et al.* 2009). Interestingly, the loss or gain of specificity was not directly tied to changes in interaction strength with Pbs2 (Figure 3c). Mutants that caused gains in specificity were associated with both significant increases and decreases of Sho1-Pbs2 interaction strength, although the two mutants that cause loss of specificity only (P97A and L98F) are associated with decreases of interaction strength. Intriguingly, there seems to be a position dependent effect, as all specificity increasing mutations are outside the core motif - though not necessarily outside the extended motif - while both mutations that only decrease specificity are situated in the heart of the core motif. Different selection pressures may be acting on residues depending on their proximity to the binding motif.

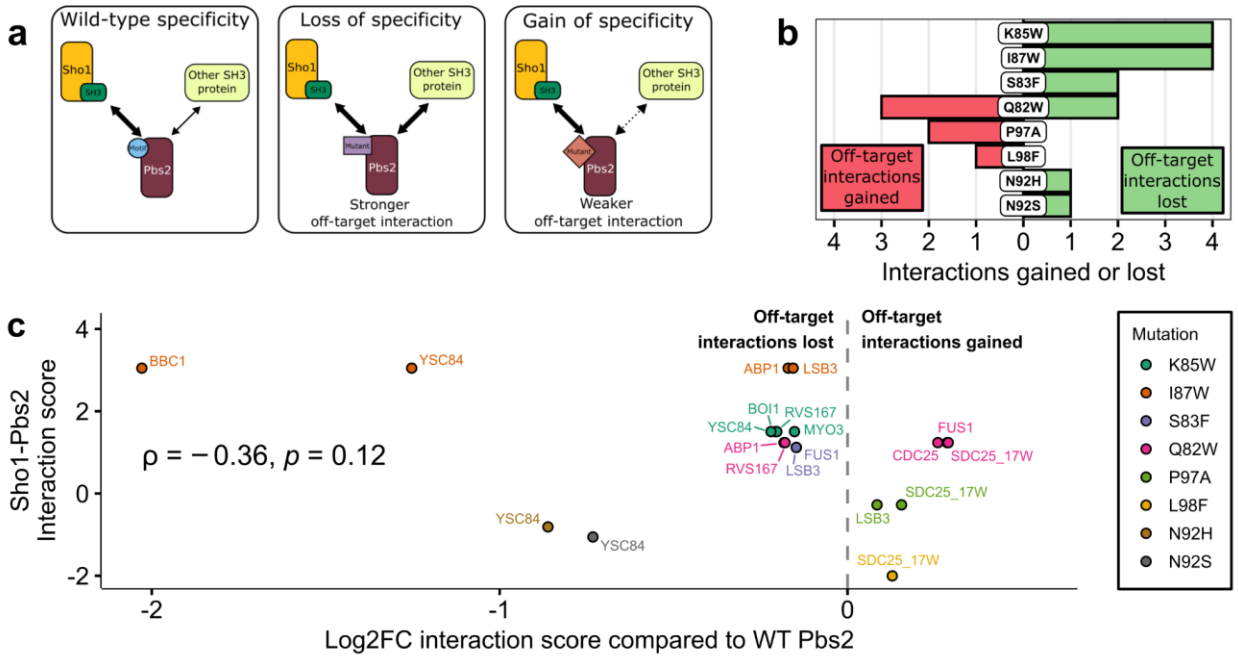

Figure 3. A few mutations cause changes to Pbs2 binding specificity

a) When a Pbs2 mutant interacts more strongly than wild-type Pbs2 with non-Sho1 SH3 domain containing proteins, there is a specificity loss, due to the stronger off-target binding. Conversely, when a Pbs2 mutant interacts less strongly than wild-type Pbs2 with

non-Sho1 SH3 domain containing proteins, there is a specificity gain, as there is now weaker off-target binding.

b) Summary of specificity gains and losses, based on the DHFR-PCA on solid media of Pbs2 mutants interacting with all SH3 domain containing proteins in yeast. On the right are indicated in green the number of SH3 domain containing proteins for which the mutant Pbs2 interaction is significantly weaker than wild-type Pbs2, and on the left is indicated in red the number of SH3 domain containing proteins for which the mutant Pbs2 interaction is significantly stronger (Welch's t-test with false discovery rate corrected p-value < 0.05).

c) Scatterplot of Pbs2 mutants' interaction scores with Sho1, and their specificity of binding to Sho1. The specificity is defined as the log2-fold change of the Pbs2 mutant interaction score with a given SH3 domain containing protein and of the wild-type Pbs2 interaction score with the same protein. The SH3 domain containing proteins are indicated next to the points, and the Pbs2 mutants are identified by their color. The specificity measurement data is from the solid DHFR-PCA, while the interaction score is from the validation assay on individually reconstructed mutants for all mutants except for Q82W and S83F, which were not included in the validation assay, so the measurements are from the DHFR-PCA on the DMS library of the region surrounding the motif. The correlation is weak and non-significant, with a spearman's rho of -0.36 and a p-value of 0.12.

Structure prediction suggests a secondary contact between extended motif and Sho1

A crystal structure of the SH3 domain of Sho1 in complex with a 9 residue-long segment of Pbs2 reveals that the core motif occupies the entirety of the canonical binding pocket of Sho1 (Kursula *et al.* 2008). However, many mutations outside the core motif have a strong effect on binding and specificity. The non-core-motif residues must affect the interaction of Pbs2 with Sho1 and other SH3 domains, but it is unclear how. One possibility is that the residues in the extended motif are interacting with Sho1 outside of the canonical binding pocket. This would not be unprecedented, as an NMR structure of the SH3 domain of the human protein Src interacting with long peptides revealed interactions involving residues outside of the canonical binding pocket, which increased the strength and specificity of the interaction (Rickles *et al.* 1995; Feng *et al.* 1995). No experimentally determined structure has been measured for the entirety of Sho1 or Pbs2, so we turned towards structure predictions using AlphaFold-Multimer (Jumper *et al.* 2021; Evans *et al.* 2022) to determine if binding outside the canonical binding pocket was conceivable (Figure S11).

By modeling the entire Sho1 protein along with the surrounding region of the Pbs2 motif (positions 71-126), we found potential interactions outside of the canonical binding pocket of Sho1, mediated by residues outside the core motif of Pbs2 (Figure 4a). In the predicted model, a hydrophobic pocket is formed between the SH3 domain and a loop of Sho1, which interacts with an alpha helix composed of Pbs2 positions 84 to 92 (Figure 4b). Interestingly, all but one of the mutants which significantly increase interaction strength are found in the positions comprising the helix. To help explain how different mutations could modify binding, we predicted the structures of the 5 Pbs2 variants with the strongest interaction strength with Sho1, using the same method as with wild-

type Pbs2. In particular, I87W, which is the strongest interacting mutant measured, positions its side-chain such that it interacts with the hydrophobic pocket, and additionally forms a hydrogen bond with the aspartic acid in position 333 of the Sho1 sequence, potentially explaining its strong interaction strength relative to all other Pbs2 variants (Figure 4c). Only 2 other SH3 domains in yeast have an aspartic acid at the same relative position (Dionne *et al.* 2021), which could explain how I87W gains specificity to Sho1, as it forms interactions that are nearly only possible with Sho1. Of the other variants tested, H86W, V91L and V91M all place a hydrophobic side chain in the hydrophobic pocket, potentially strengthening the interaction, while the side chain of Q89D faces away from the hydrophobic pocket, thus the reduced hydrophobicity does not interfere with the interaction (Figure S12).

We further reasoned that substituting a non-hydrophobic residue in one of the Pbs2 positions which is predicted to contact the hydrophobic pocket could interrupt this interaction, and weaken the affinity. Indeed, when classifying the mutations in the alpha helix by their hydrophobicity (Monera *et al.* 1995), we find that hydrophobic residues in positions 87, 90 and 91 strengthen the interaction, while most non-hydrophobic residues in these positions reduce the interaction strength (Figure 4d). We reasoned that these are positions that situate their side chains in the hydrophobic pocket. While only predictions, these models are consistent with our results and suggest that residues outside the core motif of Pbs2 can interact directly with Sho1, thus they have the capacity to modulate affinity and specificity.

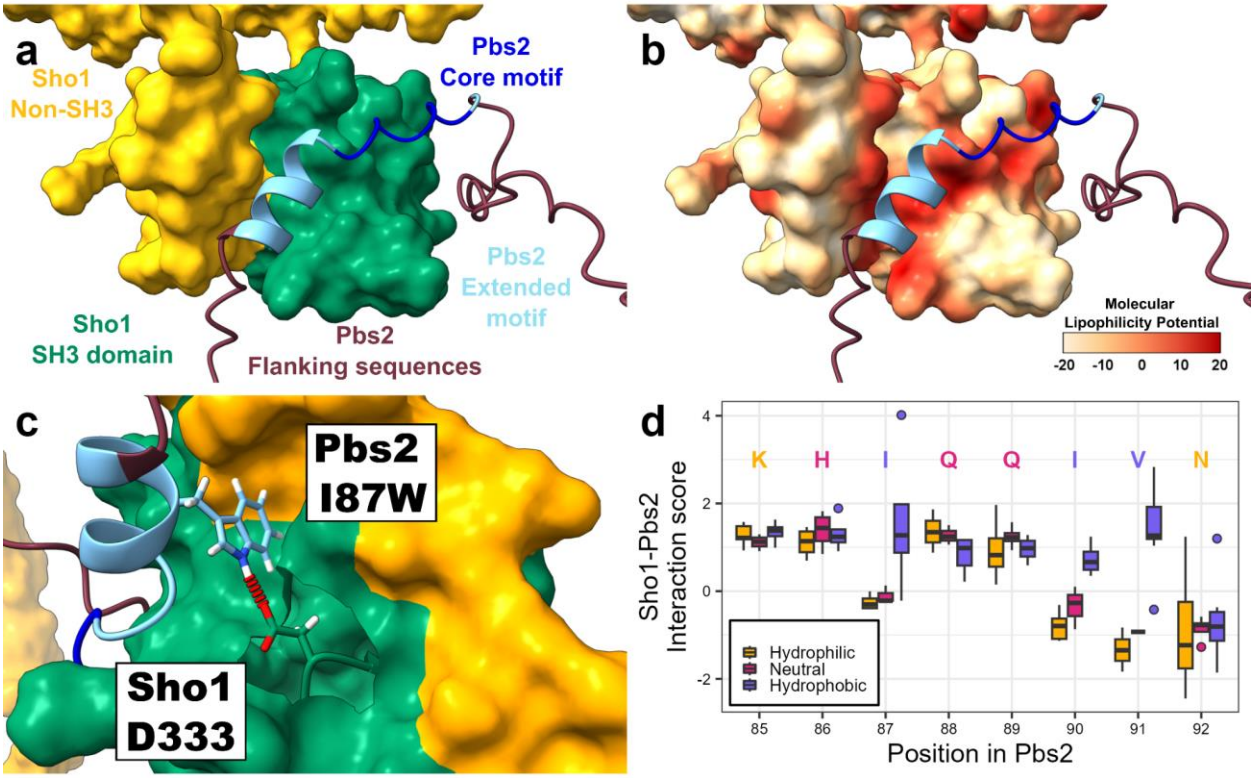

Figure 4. Contacts mediated by positions outside the core motif of Pbs2 could modulate binding

a) Structure of Sho1 in complex with residues 71 to 126 of Pbs2 predicted with AlphaFold2-Multimer (Jumper *et al.* 2021; Evans *et al.* 2022). The structure is positioned to show the helix on Pbs2 interacting with a hydrophobic pocket on Sho1. The structure is colored by the different regions of Sho1 and Pbs2, as indicated on the panel.
b) Hydrophobicity map of the predicted structure of Sho1, with high molecular lipophilicity potential (MLP) indicating a hydrophobic surface, and low MLP indicating a hydrophilic surface. MLP calculated using Chimera X 1.6.1. Coloring of Pbs2 as in panel a).
c) Close-up of the predicted structure of Sho1 with residues 71 to 126 of Pbs2 with mutation I87W. The side-chain of W87 is shown, and a hydrogen bond (red dotted line) is predicted with D333 of Sho1. Coloring of the proteins is as described in panel a).
d) Boxplot of interaction scores of Pbs2 mutants from the DHFR-PCA of the DMS library of the extended motif, based on the hydrophobicity of the substituted residue. The wild-type residue of Pbs2 for every position is indicated and colored according to its hydrophobicity. Nonsense mutants are not included in this analysis. Hydrophobicity for the different amino acids was obtained from (Monera *et al.* 1995), and F, I, W, L, V, M, Y, C, and A were classified as hydrophobic, T, H, E, S and Q were classified as neutral and R, K, N, G, P and D were classified as hydrophilic.

Discussion

Binding motifs face the double challenge of binding their partner with appropriate strength while avoiding spurious interactions with non-canonical binding partners. We set out to explore the interplay between these two phenotypes using a canonical yeast signaling pathway as a model. Using deep mutational scanning libraries of the Pbs2 binding motif and its surrounding sequences, we measured the impact of single residue mutations on interaction strength with Sho1. We also measured the interaction of selected Pbs2 mutants with all SH3 containing proteins in the cell, allowing us to detect gains or losses of specificity. We found that there is no strong and systematic relationship between these two factors, which suggests that they can be independently modified.

One important consideration in domain-peptide interactions is the potential trade-off between interaction affinity and specificity. Previous studies on SH2 and PDZ domains, both domains that bind short motifs similarly to SH3 domains, have put forth that mutants which bind with higher affinity also possess lower specificity (Ernst *et al.* 2010; Haslam and Shields 2012; Kaneko *et al.* 2012; Karlsson *et al.* 2016), suggesting that high affinity and high specificity are incompatible. This represents an intuitive idea: a protein capable of having strong interactions with a certain motif will also have more frequent and stronger spurious interactions with motifs of the same family, which are physically and chemically similar. On the other hand, a computational assay studying binding motifs, including SH3 binding motifs, found that an increase in affinity can lead to an increase in specificity (Kelil *et al.* 2016). The latter case more closely matches what we

observe with the Pbs2 motif and its surrounding region when measuring interactions in living cells, as loss of specificity does not occur in the strongest binding mutants. Moreover, the studies suggesting incompatibility between affinity and specificity have focused on engineered versions of binding domains, and not on the binding motifs, and have tested binding *in vitro* using phage display methods with isolated domains and peptides. Other works have emphasized the importance of the residues surrounding the core motif — in this case defined as K/RXXPXXP, corresponding to positions 93 to 99 of Pbs2 — in determining both affinity and specificity (Li 2005; Ivarsson and Jemth 2019). In fact, another study found that nearly 30% of binding energy from the binding motif was contributed by non-core-motif residues, and suggests that the residues in what we call the extended motif mostly play a role in determining specificity (Stein and Aloy 2008). In our experimental work, we found that all mutations which significantly increase the interaction strength between Sho1 and Pbs2 are situated outside of the core motif, as are the mutations that increase specificity. Conversely, P97A and L98F, the two mutants which solely reduce specificity, are found in the core motif, between the two conserved prolines. These two specificity loss mutations also significantly reduce the interaction strength with Sho1.

According to our data, the wild-type core motif could be already optimized for the strongest possible interaction strength. This signifies that for mutations in the core motif we are limited to measuring potential trade-offs between affinity and specificity caused by losses of affinity, and we can not test whether a gain in affinity is tied to a decrease in specificity. All this suggests different roles for the core and extended motif in determining affinity and specificity, with core motif residues more constrained, while residues in the extended motif are less constrained and able to increase affinity and specificity when mutated.

Previous work on interaction domains has shown that SH3 domain mediated interactions are context specific, meaning that the properties of the interactions depend not only on the domain itself, but also on the protein context. This context can be composed of many factors, including the non-SH3 sequence of the protein, other proteins interacting with the SH3 containing protein, and cellular localization (Dionne *et al.* 2022). SH3 mediated interactions therefore do not simply depend on the SH3 sequence. For example, when inserting an SH3 domain into a different protein or expressing an SH3 domain without its host protein, the SH3 domain's interaction profile substantially changes (Dionne *et al.* 2021; Lemieux *et al.* 2024; Dibyachintan *et al.* 2024). Thus, Pbs2 mutations may increase or decrease binding strength not only with the Sho1 SH3 domain, but also with the Sho1 context. It is unclear how Pbs2 mutations could modulate binding with the Sho1 context, although this could involve stereochemical adjustments of SH3 binding loops or changes which contribute to stabilizing or destabilizing interactions with other Sho1 binding partners. There are observations of other proteins, namely Ste11 and Ste50, interacting with the Sho1 SH3 domain outside of the canonical binding pocket (Zarrinpar *et al.* 2004; Tatebayashi *et al.* 2006). Changes to the Pbs2 peptide may affect the stability of the interaction of these proteins, which are also involved in the osmotic stress response pathway.

One interesting possibility that may explain the higher binding strength conferred by certain residues outside the core motif is that the mutated residues may interact with either residues outside the canonical binding pocket on the SH3 domain or even with non-SH3 surfaces on Sho1. All the mutations which increased interaction strength and specificity were found to be outside of

the core Pbs2 motif. These mutations are not in the portion of the motif which fits in the canonical binding pocket of Sho1, meaning that they must form interactions with some other surface. Non-binding pocket interactions have previously been observed in multiple SH3 mediated interactions (Dalgarno *et al.* 1997; Li 2005; Gaussmann *et al.* 2024), including one case where residues distal to the motif also interacted with the SH3 domain (Lee *et al.* 1996). Using predicted protein complex structures generated by AlphaFold-Multimer, we were able to hypothesize that a hydrophobic pocket is formed between the SH3 domain and a non-SH3 loop of Sho1, which residues of the extended motif can fill. The presence of such a pocket can explain the increased affinity of many Pbs2 mutants in the extended motif, as predicted structures of these models show that substituted hydrophobic side chains can insert themselves into the pocket. Perhaps the flexible structure of Pbs2 can place itself in such a way to maximize the hydrophobic interaction between any mutated side chain and the hydrophobic pocket. These predicted structures may represent only one possible form of the Sho1-Pbs2 interaction, which may in reality be dynamic due to the disordered nature of the region surrounding the Pbs2 motif. Nevertheless, they offer a potential example of non-core motif mediated binding, and propose a new model of increasing affinity and specificity. By removing the need for affinity to be dependent only on the canonical SH3 binding pocket, this proposed model allows binding to Sho1 surfaces which are less conserved among SH3 domains, and thus easier to differentiate. Perhaps the most striking example of this is the strongest interacting mutant, I87W. This mutation is predicted to form a hydrogen bond with an aspartic acid residue that is not conserved among SH3 domains in yeast. The hydrophobic pocket formed by both SH3 and non-SH3 parts of Sho1 may represent another structural feature which may help differentiate Sho1 from other SH3 domains, and allow increased affinity to develop in Pbs2 without increasing the affinity to other SH3 containing proteins. The proposed model of binding also involves a larger number of residues in tuning affinity and specificity, potentially uncoupling affinity and specificity and therefore avoiding a trade-off between these two phenotypes. Affinity and specificity may only be linked for highly conserved residues and structures, such as the core motif or the canonical SH3 binding pocket, but for less constrained residues, may develop independently.

Previous work has already focused on the binding of Pbs2 motif variants (Zarrinpar *et al.* 2003). This study led to an initial proposition of negative selection in protein interaction networks. We replicate some of the findings of this previous work, for example, showing that mutations near the Pbs2 motif can cause both gain and loss of binding strength. This work also suggested that loss of specificity could be deleterious to the cell. While we do not find any significant loss of cell proliferation for mutants with loss of specificity, mutant I87W, which is the strongest interacting mutant, does seem to have a small negative effect on the cell (Figure S9). However, I87W also increases specificity. If I87W truly has a deleterious effect on the cell, it is not through loss of specificity. In other pathways, mutations which increase affinity have been found to have deleterious effects, by reducing the dynamicity of the pathway, and impeding dissociation of the partners (Wang *et al.* 2018). For the Sho1-Pbs2 interaction, previous work has found that a mutation in the Sho1 SH3 domain that increased affinity also led to a small reduction in cell growth (Marles *et al.* 2004), indicating that the wild-type affinity is probably already optimized, and that stronger binding may disrupt signaling.

However, many results in the previous work exploring the specificity of Pbs2 variants are substantially different from what is reported here. Foremost, this previous study finds no Pbs2 variant has wild-type-like specificity, and that many Pbs2 mutants interact with other yeast SH3 domains. We find most mutants have specificity comparable to wild-type Pbs2, and identify 5 that are more specific. The experimental approach used could explain this difference in results. While our interaction measurements were all done *in vivo* using the DHFR protein complementation assay, in the previous work affinity and specificity measurements were done *in vitro* using purified SH3 domains and a 10 residue peptide of Pbs2 variants. The difference between interactions detected *in vivo* and *in vitro* is not surprising, as a manual curation of the literature found that of 40 SH3 mediated interactions identified *in vivo* only 40% were also detected *in vitro* (Kelil *et al.* 2017). Our results also suggest a role for non-core-motif residues of Pbs2 in determining affinity and specificity, and a potential for binding non-SH3 surfaces of Sho1. The impact of *in vivo* binding and the non-core motif could not have been measured by using only 10 residue long Pbs2 fragments and purified SH3 domains, and in general any contribution by the protein context of either Sho1 or Pbs2 would not have been captured. Another major difference is that mutant strains in the previous work in which growth on high osmolarity media was tested have a double deletion of *SSK2* and *SSK22*, which inactivates a redundant branch of the HOG signaling pathway, that can phosphorylate Hog1 independently of Sho1 and Pbs2 binding (Zarrinpar *et al.* 2003; Saito and Posas 2012). With the deletion of the redundant pathway branch, the Sho1 mediated pathway becomes the only osmotic stress response mechanism in the cell. While this deletion makes phenotypes easier to observe, it may also exaggerate the effects of Pbs2 mutations. It should also not affect the Sho1-Pbs2 interaction.

In conclusion, we show that mutations in the region surrounding the binding motif of Pbs2 can both increase and decrease binding strength and specificity with Sho1. The lack of correlation between these parameters suggests that they can be independently optimized, and that high affinity does not necessarily lead to lowered specificity. We also propose a role for non-core-motif residues in increasing binding affinity and specificity independently of binding in the canonical SH3 binding pocket. While our findings only apply to the Sho1 binding motif of Pbs2, the lessons learned here could be used to better understand binding by SH3 domains and other globular binding domain families. A more thorough characterization of binding motifs will be necessary before these conclusions are generalizable to other binding domain motifs.

Methods

Growth conditions

Escherichia coli cells were grown in 2YT medium (1% yeast extract, 1.6% tryptone, 0.2% glucose, 0.5% NaCl, and 2% agar for solid plates) with shaking at 37 °C for liquid cultures. When specified, 100 µg/mL of ampicillin (Amp, Bioshop Canada) were added as a selection agent. *Saccharomyces cerevisiae* cells were grown in YPD medium (1% yeast extract, 2% tryptone, 2% glucose, and 2% agar for solid plates), synthetic complete medium buffered to a pH of 6.0 (0.174%

yeast nitrogen base without amino acids, without ammonium sulfate, 2% glucose, 0.134% amino acid dropout complete, 0.1% monosodium glutamate, with 1% succinic acid and 0.6% NaOH as buffer) or PCA medium (0.67% yeast nitrogen base without amino acids and without ammonium sulfate, 2% glucose, 10% liquid drop-out without adenine, methionine, and lysine, and 200 µg/ml methotrexate (MTX, Bioshop Canada) diluted in dimethyl sulfoxide (DMSO, Bioshop Canada), and 2.5% noble agar for solid plates), as specified. When specified, 200 µg/mL of G418 (Bioshop Canada), 100 µg/mL of nourseothricin (Nat, Jena Bioscience) or 250 µg/mL of hygromycin B (Hyg, Bioshop Canada) were used as selection agents. Also when specified, 1 M of sorbitol (Bioshop Canada) was added to either liquid or solid PCA medium. Yeast cultures were grown at 30 °C with agitation at 250 rpm. See Table S1 for details of all growth media used.

Cloning

All plasmids were constructed by Gibson assembly. As template for the *PBS2* DMS library construction (pUC19-Pbs2, see below), a pUC19 plasmid backbone was amplified (Addgene #50005, primers 1F and 1R, all primers detailed in Table S2), then digested for 1 hour at 37 °C using SacI (New England Biolabs). This linearized plasmid was used for Gibson assembly with an insert composed of a 248 base pair region of *PBS2* amplified from genomic DNA, using primers that add homology arms (Primers 2F and 2R). For the CRISPR-Cas9 based insertion of sequences, the pCAS plasmid (Addgene #60847) was modified as previously described (Ryan *et al.* 2016) to change the sgRNA to target either the Sho1 binding motif of Pbs2 (pCAS-Pbs2, primers 3F and 3R), the SH3 domain of Sho1 (pCAS-Sho1, primers 4F and 4R), or the stuffer sequence which was inserted into *PBS2* (pCAS-stuffer, primer 5F and 5R) (Dionne *et al.* 2021). Proper plasmid construction was verified using Sanger sequencing (Primers 6F and 6R) (Messing 1983).

Strain construction

All strains used are summarized in Table S3. Yeast strains were constructed with either the F[1,2] or the F[3] fragments of an engineered murine DHFR protein fused to different proteins, to measure protein interaction strength as previously described (Tarassov *et al.* 2008; Michnick *et al.* 2016). The transformed sequence contains the DHFR F[1,2] fusion sequence as well as a nourseothricin resistance cassette, or the DHFR F[3] fusion sequence with a hygromycin B resistance cassette. This allows selection of the strains with DHFR fragment fusions. The DHFR F[1,2] tagged strains were derived from MATa strain BY4741 (*his3Δ leu2Δ met15Δ ura3Δ*), while the DHFR F[3] strains were derived from MATα strain BY4742 (*his3Δ leu2Δ lys2Δ ura3Δ*). The Hog1-DHFR F[1,2] strain and the Pbs2-DHFR F[3] strain used in the paper were taken from the Yeast Protein Interactome Collection (Horizon Discovery) (Tarassov *et al.* 2008). The Sho1-DHFR F[1,2] strain additionally had a 1X FLAG tag at the end of the fragment construct, and its construction was described in a previous publication (Dionne *et al.* 2021). Briefly, the DHFR F[1,2], the Nat cassette, a flexible linker and the FLAG tag sequence were amplified from the pAG25-DHFR F[1,2]-linker-FLAG plasmid (Dionne *et al.* 2021) using primers with homology arms matching the regions either side of the *SHO1* termination codon. The cassette was transformed into BY4741 cells and integrated by homologous recombination. Further deletions were done in the DHFR F[1,2] tagged strains in order to knock out *PBS2*, using the *LEU2* cassette from pUG37 (Gueldener *et al.* 2002), through homologous recombination (Primers 7F and 7R). Proper deletion

was verified by PCR (Primers 8 to 11) and sequencing (Gueldener *et al.* 2002). After the mating of the DHFR F[1,2] MATa strains with the Pbs2-DHFR F[3] MATα, only one copy of *PBS2* is present. This prevents the additional wild-type allele from influencing the measurements of interaction strength of the variants.

The Pbs2 mutants of interest for the DHFR-PCA growth curves were constructed from the Pbs2-DHFR F[3] fusion strain. First, the region surrounding the Sho1 binding motif of Pbs2 (codons 71 to 126) was replaced with a stuffer sequence (GGCGGAAGTTCTGGAGGTGGTGGT) that translates into a flexible linker sequence (GGSSGGGG), by co-transformation of the pCAS-Pbs2 plasmid, and of a repair template consisting of the stuffer sequence flanked by homology arms matching the sequences around codons 71 to 126 of *PBS2* (produced by amplifying the stuffer sequence with primers 12F and 12R), following a previously published protocol (Ryan *et al.* 2016). This produced the Pbs2-stuffed-DHFR F[3] strain, which was used for the construction of the individually reconstructed mutants as well as for the construction of the DMS libraries (see below). The individually reconstructed mutants contain all mutants used in a previous paper exploring Pbs2 mutants (Zarrinpar *et al.* 2003), including a P94A+P97A double mutant. The mutants were individually constructed by co-transforming the Pbs2-stuffed-DHFR F[3] strain with the pCAS-stuffer plasmid targeting the aforementioned stuffer, and synthesized oligonucleotide sequences corresponding to the desired mutation (Integrated DNA Technologies) (Table S4). The stuffed strain as well as all reconstructed strains were verified by PCR and Sanger sequencing (Primers 13F and 13R). The pCAS plasmids were purged by growth in liquid YPD without G418, and loss of the plasmid was verified by lack of growth on YPD+G418 plates.

For the extended motif DMS library and the individually reconstructed mutants used in the validation competition assays, three additional haploid strains were built, into which Pbs2 mutations were inserted. The first two strains were Hog1-DHFR F[1,2]/Pbs2-stuffed-DHFR F[3] and Sho1-DHFR F[1,2]/Pbs2-stuffed-DHFR F[3]. These were built by adding the DHFR F[1,2] tag to either *HOG1* or *SHO1* in the MATα Pbs2-stuffed-DHFR F[3] strain previously constructed. The DHFR F[1,2] moieties were amplified from plasmid pAG25-DHFR F[1,2]-linker-FLAG plasmid using primers with homology arms to either the *HOG1* or *SHO1* locus (Primers 14 F to 15R) (Dionne *et al.* 2021). Proper tagging was verified using PCR and Sanger sequencing (Primers 16 to 18) (Freschi *et al.* 2013; Dionne *et al.* 2021). The third strain was Pbs2-stuffed, which was used to measure the proliferation of mutants without the effect of the DHFR fragment. This was constructed in the haploid strain BY4742, using the same strategy to insert the stuffer into *PBS2* as detailed above.

The selected Pbs2 mutants for the validation assay were constructed in these three same strains by transformation with repair templates containing the mutations of interest, formed through fusion PCR. Briefly, forward and reverse primers were designed for each mutant to be constructed, which contained the mutated sequence instead of the wild-type sequence (Primers 19F to 110R). These primers were used for separate PCR amplification of the *PBS2* sequence along with either common forward or reverse primers (Primers 111F and 111R), to create two overlapping fragments. These were combined in a second PCR using only the two common primers, which fused the overlapping sequences together, to create a single fragment of 338 base pairs, which

was identical to *PBS2* except for the mutated codon of interest. These fragments were transformed into DHFR F[1,2]/Pbs2-stuffed-DHFR F[3] strains using the CRISPR-Cas9 strategy described above. Mutants were confirmed by PCR and sequencing (Primers 112F and 112R). Most mutations were constructed in all three DHFR strains, but a certain number could only be built in one or two of the strains. The successfully constructed mutants are listed in Table S3.

For the DHFR-PCA screen on solid media, the Pbs2 mutant strains used in the DHFR-PCA growth curves and constructed using synthesized oligonucleotide sequences were used. The SH3 containing proteins DHFR F[1,2] strains were obtained from the Yeast Protein Interactome Collection (Horizon Discovery). A version of Sho1 was also built where the entire SH3 domain was replaced by the same flexible stuffer used in the Pbs2-stuffed strain. As with Pbs2, the stuffer was amplified using primers adding homology to the flanking sequences of the Sho1 SH3 domain locus (Primers 113F and 113R). The stuffer was inserted into the Sho1 sequence by cotransformation of the pCas-Sho1 plasmid and the repair template of the stuffer with homology arms. Proper stuffing was verified by PCR and Sanger sequencing (Primers 114F and 114R).

<u>Construction of the surrounding region DMS library</u>

The initial DMS library covering the surrounding region of Pbs2 was constructed as previously reported (Dionne *et al.* 2021). 56 codons (168 nucleotides) were targeted, which correspond to codons 71 to 126 of the *YJL128C*/*PBS2* ORF.

A degenerate oligonucleotide was designed for each codon to be mutated, with the three nucleotides of the mutated codon replaced by an NNN codon (Primers 115 to 170). This series of 56 oligonucleotides was used to amplify pUC19-Pbs2, in a two step PCR procedure (Miyazaki 2011). At all steps, the different codons were kept in separate reactions and the mutants for each codon were created in separate reactions. In the first amplification, a megaprimer was created which includes the *PBS2* coding sequence using the degenerate oligonucleotide and a common reverse primer (Primer 171R). The megaprimer thus carries the DMS library for one codon. In the second PCR step, this megaprimer was used to amplify the entire plasmid. The PCR products were digested with DpnI (New England Biolabs) at 37°C for 1 hour to remove the original methylated template, and keep only the mutated plasmids amplified by the megaprimer. The remaining mutated amplified but unligated plasmids were transformed into chemocompetent *E. coli* cells strain MC1061, and plated on solid 2YT+Amp. The amplified plasmids were ligated and thus recircularized in the cells. All transformations resulted in hundreds of colonies and these colonies were suspended in 5 mL of 2YT. Their plasmids were extracted using a miniprep plasmid extraction kit (Presto Mini Plasmid Kit, Geneaid) to obtain a plasmid library containing all the DMS mutants. Prepared libraries were sequenced using 300-PE MiSeq technology (see DNA sequencing section), to verify that the desired codon diversity was present. Once diversity was confirmed, the libraries were amplified from the plasmids (Primers 172F and 172R), and transformed into the Pbs2-stuffed-DHFR F[3] yeast strain using the CRISPR-Cas9 strategy described in the strain construction section.

Transformed cells were plated on solid YPD+G418+Hyg for selection, and then resuspended in liquid YPD. The optical density of each suspension (each codon) was measured and all

suspensions were pooled into a masterpool, with 5 optical density units (OD) added for each codon. Frozen glycerol stocks were prepared for the individual suspensions of each codon, and multiple stocks were prepared for the masterpool. Genomic DNA was extracted from the masterpool using phenol/chloroform DNA extraction (Amberg *et al.* 2005), and as before, the library was sequenced to verify diversity. At this point, three codons had unsatisfactory diversity. A new template was created for codons 103 and 119 using fusion PCR, creating a sequence of 967 base pairs around the mutated codon, using the original degenerate primers as well as new reverse degenerate primers to create an NNN codon at either codon 103 or 119 (Primers 173 to 175). For codon 88, a new template was ordered as an oligonucleotide of 503 base pairs (Twist Bioscience), around codon 88, which is replaced by an NNN codon. These templates were transformed into Pbs2-stuffed-DHFR F[3] as described above, and diversity at the desired codon was verified with Sanger sequencing. The three supplementary cultures were pooled into the masterpool, with an OD corresponding to 1/56th of the OD of the master pool.

<u>DHFR-PCA competition assay for surrounding region DMS library</u>

The PCA selection followed a previously published protocol (Dubé *et al.* 2022). Three liquid cultures were started, each from 100 µL of the masterpool containing all mutated codon positions, in SC complete medium. These cultures were incubated at 30 °C for 16 hours. 300 µL of this preculture was mixed with 150 µL of either Sho1-DHFR F[1,2] or Hog1-DHFR F[1,2], and 1.2 mL of fresh liquid YPD. These mixes of strains were left to mate for 8 hours at 30 °C with agitation. The mated diploid cells were then selected in two successive cycles of diploid selection in liquid YPD+Nat+Hyg at 30 °C with agitation. The first cycle consisted of a 5/12 dilution of the mating culture in 3 mL of liquid YPD for 16 hours, and the second cycle consisted of a 1/10 dilution in 3 mL of liquid SC media for 24 hours. A volume equivalent to 5 OD was spun down and the supernatant was removed, to form a cellular pellet, which was stored at -80 °C. This is the initial time point used for sequencing. The selected diploid cultures were then diluted to 0.1 OD/mL in 15 mL of liquid PCA medium with either 200 µg/mL of methotrexate with 1 M of sorbitol, the same concentration of methotrexate without sorbitol, or a control without methotrexate but with 1 M sorbitol. This PCA selection was grown without light for 96 hours, except for the control cultures which were saturated after 24 hours. After this first growth cycle, the cultures were diluted 0.1 OD/mL into 15 mL of fresh liquid PCA medium, and a 5 OD pellet was spun down and stored at -80 °C. The second PCA cycle lasted the same amount of time, and at the end, as many 5 OD pellets as possible were prepared from each culture. Genomic DNA was extracted from the pellets of the second diploid selection cultures and the second PCA selection culture. The Pbs2 locus was amplified and sequenced, as described in the DNA sequencing section.

<u>Construction of the extended motif DMS library</u>

A second DMS library was constructed on the extended motif of *PBS2*, comprising codons 85 to 100. An oligonucleotide pool (Integrated Data Technologies, Table S5) was synthesized containing all possible NNK codons (K indicating either a G or T nucleotide) for the 16 codon region of interest, with homology arms for a total length of 248 base pairs. This pool was integrated into 2 different yeast strains : Sho1-DHFR F[1,2]/Pbs2-stuffed-DHFR F[3] and Hog1-DHFR F[1,2]/Pbs2-stuffed-DHFR F[3], to allow respectively for PCA measurements of Sho1-Pbs2

interaction in a haploid strain, and PCA measurements of Hog1-Pbs2 interaction in a haploid strain.

The mutant pool was integrated into these strains by replacing the Pbs2 stuffer using the CRISPR-Cas9 strategy described in the strain construction section. As before, the integrated libraries were sequenced to verify diversity. Transformed yeast libraries were stored at -80 °C.

DHFR-PCA competition assay for extended motif DMS library

The liquid PCA selection for the haploid double DHFR tagged strains was done following the same protocol as the first DHFR-PCA selection, only ignoring the mating step. However, a fourth control condition of PCA medium without methotrexate and without sorbitol was added. Three replicate pools were done for each growth condition. Frozen pellets were prepared as in the first DHFR-PCA selection.

Validation DHFR-PCA competition assay of individually reconstructed mutants

The individually reconstructed validation strains were pooled by combining 100 µL of saturated overnight culture of each mutant in YPD. 6 pools were made for each condition, three pools each from two individual reconstructed colonies of the mutant. The same conditions were used as the second liquid PCA selection: PCA medium both with and without 1 M of sorbitol and with and without methotrexate for the DHFR tagged strains. For the cell proliferation measurements, SC medium with and without 1 M of sorbitol was used. Two cycles of selection were done, with 96 hour cycles for the conditions with methotrexate and 24 hour cycles for the conditions without methotrexate, and the SC medium. Frozen pellets were prepared as for the previous liquid PCA selections.

DNA sequencing

DNA sequencing was done in generally the same manner for all experiments, with minor changes in certain cases. DNA was extracted from the frozen pellets using a standard phenol/chloroform genomic DNA extraction protocol (Amberg *et al.* 2005). The extracted DNA was amplified and barcoded using a Row-Column DNA barcoding strategy as previously described (Dubé *et al.* 2022). From the extracted genomic DNA, the *PBS2* region of interest was amplified using primers containing 3' overhangs which allow a second amplification to add barcodes (Primers 176F and 176R). PCR products were diluted 1/2500, and used as a template to add row and column barcode primers onto the sequence, with a unique combination of 5' and 3' barcodes for each replicate in each condition. The row-column barcode primers were previously described (Dubé *et al.* 2022). PCR products were migrated on an agarose gel, and DNA concentrations were estimated based on band size using the Image Lab software (BioRad Laboratories). Samples were then pooled with different volumes to obtain the same quantity of DNA from each sample. The pools were purified using magnetic beads, measured using a NanoDrop (ThermoFisher), and diluted to 0.1 ng/µL. The diluted pools were then amplified with primers adding a second set of barcodes, called plate barcodes (Dubé *et al.* 2022). These double-barcoded pools were purified on magnetic beads, and sent for sequencing on Illumina NGS machines. Unique combinations of barcodes were used to identify the DNA extracted from each pellet in each replicate of each condition. The sequencing of the first DHFR-PCA, on the larger region surrounding the Pbs2 motif

was done using Illumina NovaSeq paired-end 250 base pair technology (CHUL sequencing platform, Quebec, Canada), while all other sequencing was done using Illumina MiSeq paired-end 300 bp technology (IBIS Genomic Analysis Platform, Quebec, Canada).

After preliminary analysis of the sequencing of the DNA from the pellets of the DHFR-PCA on the extended motif DMS library, it was determined that more reads would be needed. Additional sequencing libraries were prepared fresh from the original DNA extractions. Instead of using a row-column barcoding approach, the *PBS2* region was amplified using primers (Primers 177F and 177R) with homology arms allowing the addition of Illumina Nextera barcodes (Illumina). These allow automated demultiplexing by the Illumina MiSeq instrument. All other steps were as described above.

<u>Analysis of DNA sequencing results</u>

The variant frequency in DMS libraries during construction and in the DHFR-PCA and proliferation screens was evaluated using custom scripts based on already published work (Després *et al.* 2022). Python libraries pandas 1.5.2 (The pandas development team 2023), matplotlib 3.6.2 (Hunter 2007) and numpy 1.24.1 (Harris *et al.* 2020) were used for data manipulation and visualization. Quality was assessed using FastQC 0.12.1 (Andrews 2010). Reads were trimmed using Trimmomatic 0.39 (Bolger *et al.* 2014), then demultiplexed using bowtie 1.3.1 for the sequencing of the surrounding region DMS library (Langmead *et al.* 2009), Interstellar 1.0 following the RCP-PCR configuration for the first sequencing run of the extended motif DMS library (Kijima *et al.* 2023) and cutadapt 4.7 for the validation competition assay sequencing (Martin 2011). The second sequencing run for the extended motif DMS library was barcoded using Illumina Nextera primers, and was thus automatically demultiplexed by the sequencing instrument. Forward and reverse reads were then merged using the PANDAseq software (Masella *et al.* 2012). Next, identical reads were grouped using vsearch (Rognes *et al.* 2016), and aligned to the wild-type *PBS2* sequence using the needle function from the EMBOSS software (Rice *et al.* 2000). From this, the frequency of each variant was obtained.

From the frequency of each variant, the interaction scores and selection coefficients of each variant were calculated using custom R 4.3.1 (R Core Team 2023) scripts. The R package collection tidyverse (Wickham *et al.* 2019), as well as the packages rstatix 0.7.0 (Kassambara 2021), ggpubr 0.4.0 (Kassambara 2020) and bioseq 0.1.4 (Keck 2020) were used for data analysis. R packages ggExtra 0.10.1 (Attali and Baker 2023), ggrepel 0.9.4 (Slowikowski 2023), GGally 2.2.0 (Schloerke *et al.* 2023) and cowplot 1.1.1 (Wilke 2020) were used for data visualization. Briefly, variant counts were imported, identified by the mutation type (wild type, nonsense, missense or silent) then transformed into frequencies by dividing each variant count by the total number of counts present in that sequencing library. The interaction score was calculated as the log-2-fold-change of the frequency of each variant at the end of the second cycle of methotrexate selection and the frequency of each variant after the selection for diploids (so immediately preceding the methotrexate selection). Variants were then filtered to keep only those that had 20 or more reads detected after diploid selection, in order to remove bias caused by low read counts leading to inflated scores. Next, a unique score was calculated for each variant by

taking the median score of all codons coding for the same amino acid variant in all replicates. Scores were only kept for amino acid variants that had at least 3 replicates from any combination of codons not filtered out. For the competition assay of cell proliferation, the number of generations elapsed during the selection for each replicate was calculated, as the log-2-fold-change the optical density of the cultures at the end and at the beginning of the growth cycles. The selection coefficient for each variant was calculated as follows:

$$s = \frac{ln\left(\frac{variant\ frequency\ after\ PCA\ selection}{variant\ frequency\ before\ PCA\ selection}\right) - ln\left(\frac{wt\ frequenc}{wt\ frequenc}\right.}{number\ of\ generations}$$

The frequency of the wild type used is the frequency of the wild type in the same replicate as the variant. The same filtering criteria were used for the proliferation assay as for the DHFR-PCA.

When measuring the interaction scores of the preliminary and extended motif DMS libraries, we also included control conditions without methotrexate, the selective agent allowing measurement of DHFR fragment reconstitution. The measurements in this condition should not give any information about interactions between Pbs2 and Sho1, but can inform us about any other defects in the mutant strains. We calculated DMSO scores for growth in the control condition in the same way as the interaction scores. We noticed that some nonsense mutants had growth scores comparable to wild-type Pbs2, and that some silent mutants had growth scores comparable to nonsense mutants. These abnormal scores could indicate defects in the strains, possibly resulting from the Cas9 mediated mutation process. We statistically verified which nonsense and silent mutants were abnormal by comparing every nonsense or silent mutation to all other nonsense or silent mutations (Mann-Whitney U test, $p <= 0.05$). The mutants which were significantly different were removed from the interaction score dataset. Similarly, we wanted to verify that no missense mutants had any defects caused by other sources than the interaction. We statistically verified which mutants had defects in the control condition by comparing each missense mutant to the nonsense mutants (Mann-Whitney U test with false discovery rate corrected p-value > 0.05). The missense mutants which were not significantly different from the nonsense mutants were also removed from the interaction score dataset.

We also removed from the interaction score dataset the mutants for which an abundance change was detected through gain or loss of interaction strength between Pbs2 and Hog1, as explained in the results section. Pbs2 missense mutants that had an interaction strength with Hog1 which was significantly different from wild-type Pbs2 and silent mutations (Mann-Whitney U test with false discovery rate corrected p-value $<= 0.05$), either in the presence or absence of sorbitol, were removed from the datasets.

DHFR-PCA growth curves of individually reconstructed mutants

Growth curves were measured for individually reconstructed Pbs2 mutants in DHFR-PCA medium, to validate Pbs2 interaction strength measurements. The DHFR F[3] tagged strains with the mutations were mated with a Sho1-DHFR F[1,2]/*pbs2::LEU2* strain, in order to produce diploids with complementary DHFR fusions. To mate these strains, 50 µL of precultures of each strain were mixed into 900 µL of YPD and incubated at 30 °C overnight without agitation. 2 µL of each mated culture was spotted on solid YPD+Nat+Hyg, to select for diploids. Exponential phase precultures of diploids were diluted to 0.1 OD/mL in 80 µL of PCA medium, in a 384 well plate, in 4 replicates, at 30 °C. Cultures were grown either with and without 200 µg/mL of methotrexate, and with and without 1 M sorbitol. The optical density of each well was measured every 15 minutes in a Tecan Spark plate reader (Tecan). Growth curves were analyzed using a custom script written in R (R Core Team 2023), using the tidyverse package collection (Wickham *et al.* 2019) and the R package ggpubr 0.6.0 (Kassambara 2020). A function was written to find the maximal instantaneous growth rate for each well. Mutant P94R was disregarded, as growth of all replicates in the control condition in the absence of methotrexate was much lower than all other samples, suggesting a problem with strain construction.

DHFR-PCA on solid media against SH3 domain containing proteins

The DHFR-PCA on solid media was based on previous work (Tarassov *et al.* 2008; Rochette *et al.* 2015). All colony manipulation was done using a robotic pin tool platform (BM5-SC1, S&P Robotics Inc.). The strains containing DHFR F[1,2]-tagged SH3 containing proteins were taken from the Yeast Protein Interactome Collection (Horizon Discovery). The DHFR F[3] strains containing reconstructed Pbs2 mutations were built for this project, and were the same as those used for the growth curves. Cultures were started from frozen stocks in YPD with nourseothricin for DHFR F[1,2] strains and hygromycin B for DHFR F[3] strains, in deep welled 96-well plates.

Colonies were cherry picked from the 96-well plates, and arrayed onto YPD+Nat plates for the DHFR F[1,2] strains or YPD+Hyg plates for the DHFR F[3] strains, in a 384 colony array. The DHFR F[1,2] strains were organized into a randomized pattern to avoid any effects caused by neighboring colonies. Each 384 colony plate of DHFR F[3] strains contained only copies of the same mutant. The 384 colony arrays were condensed into 1536 colony arrays on YPD+Nat or YPD+Hyg, with 4 DHFR F[3] strains per array for a total of 8 arrays, and the randomized DHFR F[1,2] pattern repeated four times. The outer two rows and columns of the 1536 arrays were LSM8-DHFR F[1,2] and CDC39-DHFR F[3], which grow well on PCA medium and serve to avoid any measurement bias from being on the edge of the array for the interactions of interest. The 1536 colony arrays were mated together by pinning the repeated DHFR F[1,2] array onto 8 YPD plates, and then pinning one of the 8 DHFR F[3] arrays onto each plate. In this collection of arrays, each interaction between an SH3 containing protein and a Pbs2 mutant was measured in 5 or 6 replicates. After 48 hours of mating at 30 °C, the mated colonies were pinned onto YPD+Nat+Hyg plates to select for diploid cells. Two growth cycles of 48 hours at 30 °C on YPD+Nat+Hyg were done. After diploid selection, the plates were photographed using an EOS Rebel T5i camera (Canon), to verify that all colonies grew correctly. The mated arrays were then pinned onto solid PCA medium plates, either with or without methotrexate, and with 1 M of sorbitol. The arrays were

grown for two cycles of 48 hours at 30 °C in a custom growth and imaging platform (S&P Robotics Inc.), which incubated the plates and took a picture of each plate every 2 hours.

Analysis of DHFR-PCA of Pbs2 mutants against SH3 domain containing proteins

First, the ImageMagick command line tool (ImageMagick Studio LLC 2023) was used to crop the images of the selection plates as well as change them to grayscale and invert the colors, using the commands: `convert -colorspace LinearGray`, `convert -crop 4200X2800+530+320` and `convert -negate`. Colony sizes were then quantified using the Python package Pyphe (Kamrad *et al.* 2020), using the command `pyphe-quantify timecourse --grid auto_1536 --t 1 --d 3 --s 0.05`. The colony sizes were analyzed and visualized using a custom script written in R 4.3.1 (R Core Team 2023), based on a previous analysis (Dionne *et al.* 2021), and using R packages from the tidyverse collection (Wickham *et al.* 2019), rstatix 0.7.2 (Kassambara 2021), ggpubr 0.6.0 (Kassambara 2020) and ggrepel 0.9.4 (Slowikowski 2023). Colony sizes were filtered, and colonies which had not grown at the end of the diploid selection were removed from the PCA results. Colony sizes were log2 transformed and then normalized by subtracting the log2- transformed median colony size for each row, column and 1536 array, including the border colonies. Scores were rescaled to fall between 0 and 1, thereby simplifying interpretation. The different replicates of the interactions were then combined, and any interactions without at least 3 replicates that grew were removed from the dataset. Then, interactions between different Pbs2 mutants and SH3 domain containing proteins were compared to the interaction between wild-type Pbs2 and the same protein, to verify which mutants interacted significantly more strongly or weakly than wild-type Pbs2 (Welch's t-test with false discovery rate corrected p-value < 0.05). The difference in interaction strength for each Pbs2 mutant with every SH3 containing protein was then calculated as the log-2-fold change between the mutant Pbs2 interaction strength and wild-type Pbs2 interaction strength. As detailed in the results sections, Nbp2 was not considered in this analysis, as it interacts with Pbs2 through a different binding site than that involved for Sho1 binding.

Structure prediction

Structure predictions were done for Pbs2 mutants in complex with Sho1 using AlphaFold 2.3.2 and the AlphaFold-Multimer implementation (Jumper *et al.* 2021; Evans *et al.* 2022). Default options were used, and only the top scoring model for each mutant was relaxed. For Sho1, the sequence of the entire protein was used for prediction (Uniprot entry P40073). For Pbs2, residues 71 to 126 were used for the prediction (Uniprot entry P08018). Predicted structures were visualized using ChimeraX 1.6.1 (Pettersen *et al.* 2021).

Data availability

Strains and plasmids are available upon request. All analysis scripts and visualization scripts are available on Github at the following address: https://github.com/Landrylab/Jordan_et_al_2024. All data, including demultiplexed sequencing data, results from the DHFR-PCA experiments, growth

curve data, predicted structures and all files and information necessary to run the scripts are available in the following Dryad repository: https://doi.org/10.5061/dryad.79cnp5j3z.

Acknowledgments

The authors thank Philippe C. Després, Moïra Dion and Dan Evans-Yamamoto for help with sequencing data analysis. We also thank all members of the LandryLab team for thoughtful comments on the experiments and on figure conception. All molecular graphics were performed using USCF ChimeraX. The protein structure predictions were enabled by computing resources provided by the Digital Research Alliance of Canada.

Funding

This work was supported by Canadian Institutes of Health Research Foundation grant number 387697 and Human Frontier Science Program research grant RGP34/2018 to CRL. C.R.L. holds the Canada Research Chair in Cellular Systems and Synthetic Biology. D.J. was supported by the Canada Graduate Scholarship - Master's program from NSERC, a graduate scholarship from PROTEO, a graduate scholarship from the NSERC CREATE program EvoFunPath, a Postgraduate Scholarship - Doctoral from NSERC and a Doctoral scholarship from FRQS. D.B. was funded by the EMBO Long-Term Fellowship (LTF) (ALTF 1069-2019). U.D. was funded by an NSERC graduate fellowship.

Author contributions

All authors were involved in the design of the study. C.R.L. directed this work and obtained funding. D.J. and A.K.D. performed the experiments. D.J. performed the computational analyses. D.J. wrote the first draft of the manuscript. All authors contributed to revising and writing the final version of the manuscript.

Supplementary Figures

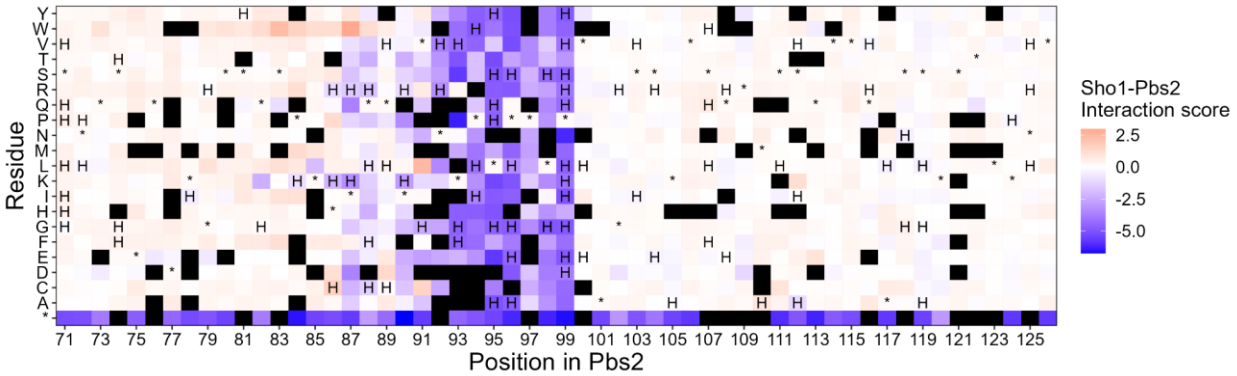

Figure S1.
Sho1-Pbs2 interaction scores for Pbs2 mutants in the DHFR-PCA on the DMS library of the region surrounding the Pbs2 motif. Scores are indicated for each mutant according to their position in Pbs2 and the residue that it was mutated to. The wild-type residue for each position is indicated by an asterisk (*). Mutants which significantly affect the Hog1-Pbs2 interaction are marked with the letter H (Mann-Whitney U test with false discovery rate corrected p-value < 0.05). Mutants which were removed from the dataset for having too few reads in the initial timepoint are marked in black.

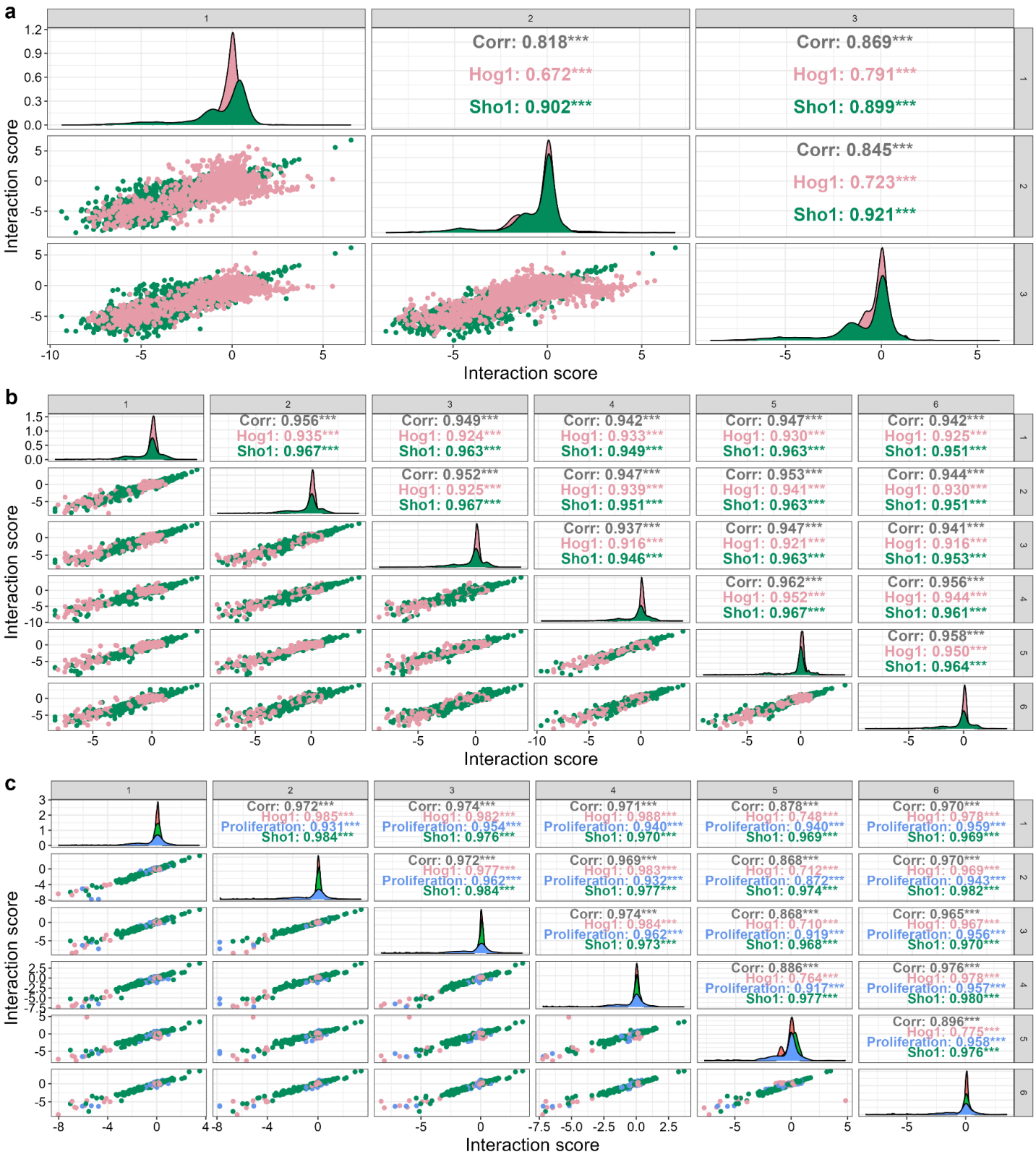
a
Corr: 0.818***
Hog1: 0.672***
Sho1: 0.902***
Corr: 0.869***
Hog1: 0.791***
Sho1: 0.899***
Corr: 0.845***
Hog1: 0.723***
Sho1: 0.921***
Interaction score
b
Corr: 0.956***
Hog1: 0.935***
Sho1: 0.967***
Corr: 0.949***
Hog1: 0.924***
Sho1: 0.963***
Corr: 0.942***
Hog1: 0.933***
Sho1: 0.949***
Corr: 0.947***
Hog1: 0.930***
Sho1: 0.963***
Corr: 0.942***
Hog1: 0.925***
Sho1: 0.951***
Corr: 0.952***
Hog1: 0.925***
Sho1: 0.967***
Corr: 0.947***
Hog1: 0.939***
Sho1: 0.951***
Corr: 0.953***
Hog1: 0.941***
Sho1: 0.963***
Corr: 0.944***
Hog1: 0.930***
Sho1: 0.951***
Corr: 0.937***
Hog1: 0.916***
Sho1: 0.946***
Corr: 0.947***
Hog1: 0.921***
Sho1: 0.963***
Corr: 0.941***
Hog1: 0.916***
Sho1: 0.953***
Corr: 0.962***
Hog1: 0.952***
Sho1: 0.967***
Corr: 0.956***
Hog1: 0.944***
Sho1: 0.961***
Corr: 0.958***
Hog1: 0.950***
Sho1: 0.964***
Interaction score
c
Corr: 0.972***
Hog1: 0.985***
Proliferation: 0.931***
Sho1: 0.984***
Corr: 0.974***
Hog1: 0.982***
Proliferation: 0.954***
Sho1: 0.976***
Corr: 0.971***
Hog1: 0.988***
Proliferation: 0.940***
Sho1: 0.970***
Corr: 0.878***
Hog1: 0.748***
Proliferation: 0.940***
Sho1: 0.969***
Corr: 0.970***
Hog1: 0.978***
Proliferation: 0.959***
Sho1: 0.969***
Corr: 0.972***
Hog1: 0.977***
Proliferation: 0.962***
Sho1: 0.984***
Corr: 0.969***
Hog1: 0.983***
Proliferation: 0.932***
Sho1: 0.977***
Corr: 0.868***
Hog1: 0.712***
Proliferation: 0.872***
Sho1: 0.974***
Corr: 0.970***
Hog1: 0.969***
Proliferation: 0.943***
Sho1: 0.982***
Corr: 0.974***
Hog1: 0.984***
Proliferation: 0.962***
Sho1: 0.973***
Corr: 0.868***
Hog1: 0.710***
Proliferation: 0.919***
Sho1: 0.968***
Corr: 0.965***
Hog1: 0.967***
Proliferation: 0.956***
Sho1: 0.970***
Corr: 0.886***
Hog1: 0.764***
Proliferation: 0.917***
Sho1: 0.977***
Corr: 0.976***
Hog1: 0.978***
Proliferation: 0.957***
Sho1: 0.980***
Corr: 0.896***
Hog1: 0.775***
Proliferation: 0.958***
Sho1: 0.976***
Interaction score

1064

Figure S2.

Correlation between replicates in the DHFR-PCA experiments on DMS libraries of the Pbs2 binding motif a) Scatterplot between the 3 replicates of DHFR-PCA interaction scores for mutants in the DMS library of the surrounding region of the Pbs2 motif. Each point represents one Pbs2 codon variant in one condition (with or without sorbitol, with or without MTX). The interaction partner with which the interaction score was measured is indicated by the color, with Sho1 interaction scores in green and Hog1 interaction scores in pink. The replicate number is indicated in the gray label. b) Scatterplot between the 6 replicates of DHFR-PCA interactions scores for mutants in the DMS library of only the extended motif of Pbs2. Replicates 4, 5, and 6 are sequenced from the same frozen pellets as replicates 1,2 and 3, but from a separate sequencing run. Each point represents one Pbs2 codon variant in one condition (with or without sorbitol, with or without MTX). The interaction partner with which the interaction score was measured is indicated by the color, as in panel a). The replicate number is indicated in the gray label.

c) Scatterplot between 6 replicates of DHFR-PCA interaction scores for individually reconstructed mutants in haploid strains. Each point represents one of the reconstructed Pbs2 mutants in one condition (with or without sorbitol, with or without MTX). The interaction partner with which the interaction score was measured is indicated by the color, as in panel a), with the exception of the blue points, which are the measurements of cell proliferation, in a strain with no DHFR tags. The replicate number is indicated in the gray label.

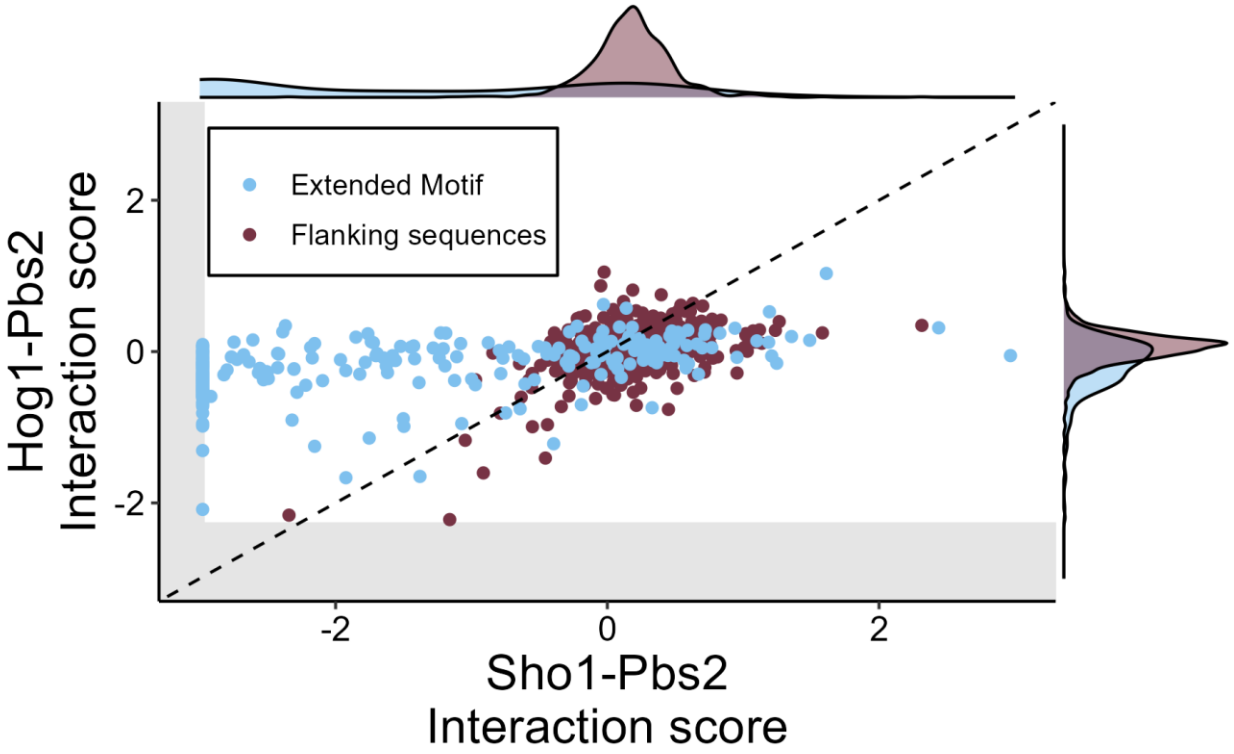

Figure S3.

Scatterplot of interaction scores for missense and silent mutants in the DMS library of the region surrounding the motif, for the interaction of Pbs2 with either Sho1 or Hog1. Points are colored according to whether the mutants are situated in the extended motif or flanking sequences. The dotted line represents the diagonal. The gray rectangles on the left and bottom of the panel represent the 97.5 percentile of scores for the nonsense variants of Pbs2, which do not express the DHFR F[3] fragment. As such, they represent the limit of detectable signal in the assay. The points which have scores comparable to the nonsense mutations, and therefore no detectable interaction, were placed at the limit of the gray rectangle to indicate that no interaction was detected. In the margins, density plots show the distribution of scores for mutants situated either in the extended motif or in the flanking sequences.

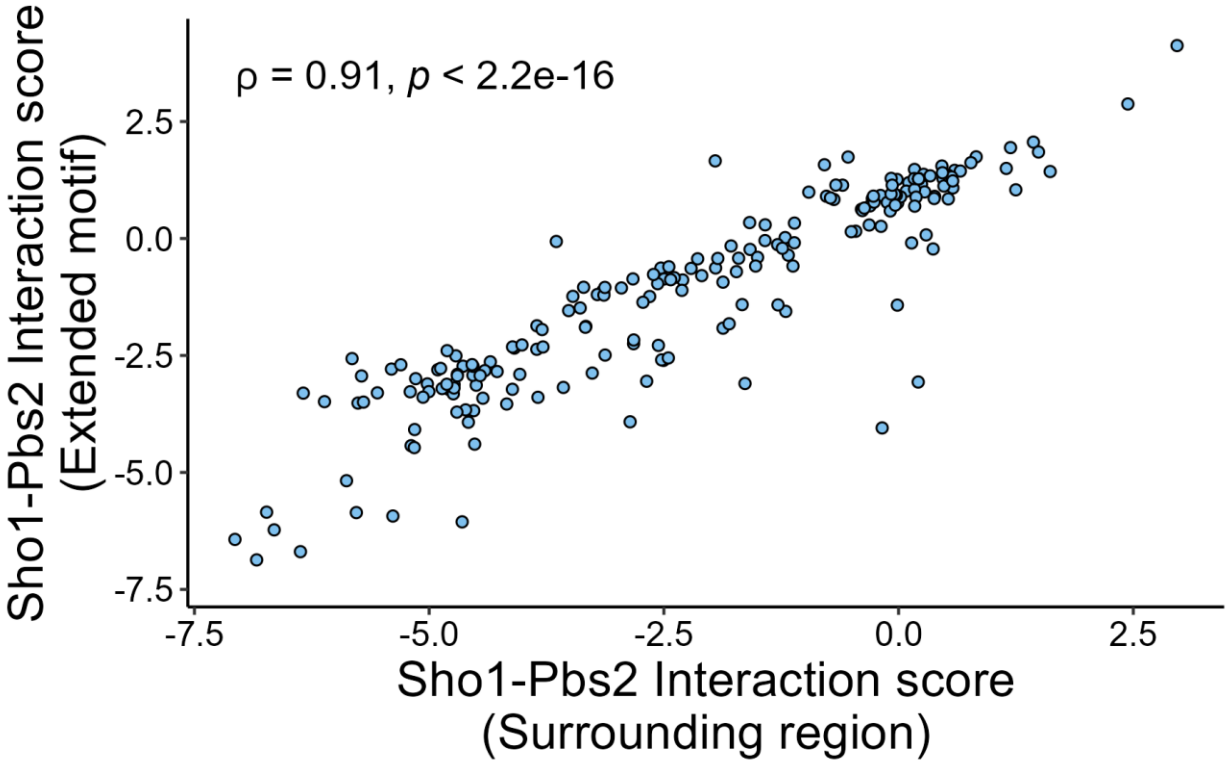

Figure S4.

Scatterplot of interaction scores of Pbs2 mutants in the initial DHFR-PCA screen on the DMS library of the surrounding region of the motif, and the subsequent DHFR-PCA screen on the DMS library of only the extended motif (positions 85 to 100). Scores shown were measured in the presence of methotrexate and 1 M of sorbitol. Spearman's rho 0.91, $p < 2.2X10^{-16}$.

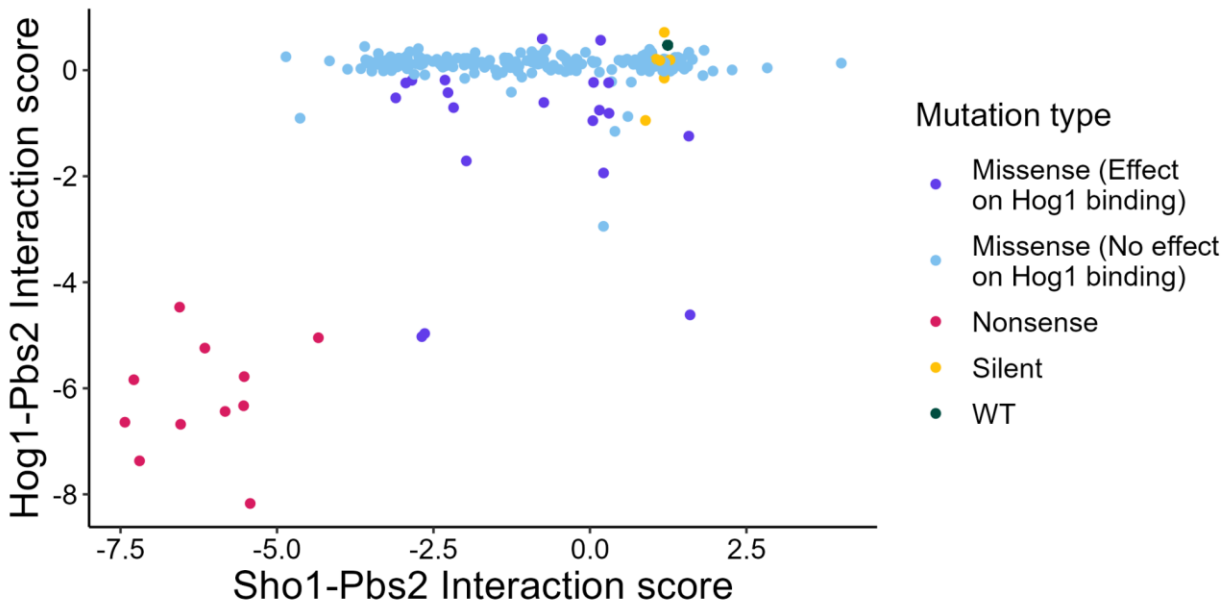

Figure S5.
Scatterplot of interaction scores of the Pbs2 extended motif DMS library mutants with Sho1 and Hog1, in the presence of 1 M of sorbitol. Purple missense points represent Pbs2 mutants which have an interaction score with Hog1 which is significantly different to the combination of silent mutants and wild-type Pbs2 (Mann-Whitney U test with false discovery rate corrected p-value < 0.05), while blue missense points represent mutants for which the Hog1 interaction score is not significantly different to the combination of silent mutants and wild-type Pbs2. The combination of silent mutations and wild type represents all mutants expressing the wild-type protein sequence. Since the Hog1 interaction is used to measure abundance and stability of the Pbs2 mutants, the significantly different mutants are considered to have an effect on the abundance or the stability of Pbs2 and were not kept for the remainder of the analysis. The only exceptions are the nonsense mutants, which were kept because they provide a useful reference.

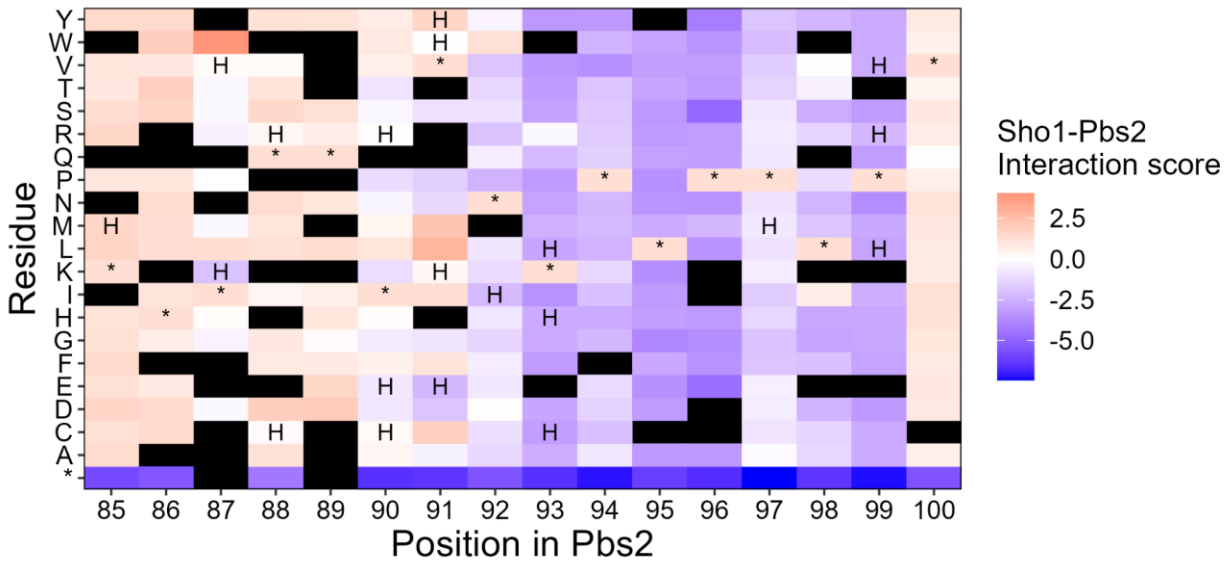

Figure S6.

Sho1-Pbs2 interaction scores for Pbs2 mutants in the DHFR-PCA on the DMS library of the extended Pbs2 motif. Scores are indicated for each mutant according to their position in Pbs2 and the residue that it was mutated to. The wild-type residue for each position is indicated by an asterisk (*). Mutants which significantly affect the Hog1-Pbs2 interaction are marked with the letter H (Mann-Whitney U test with false discovery rate corrected p-value < 0.05). Mutants which were removed from the dataset for having too few reads in the initial timepoint are marked in black.

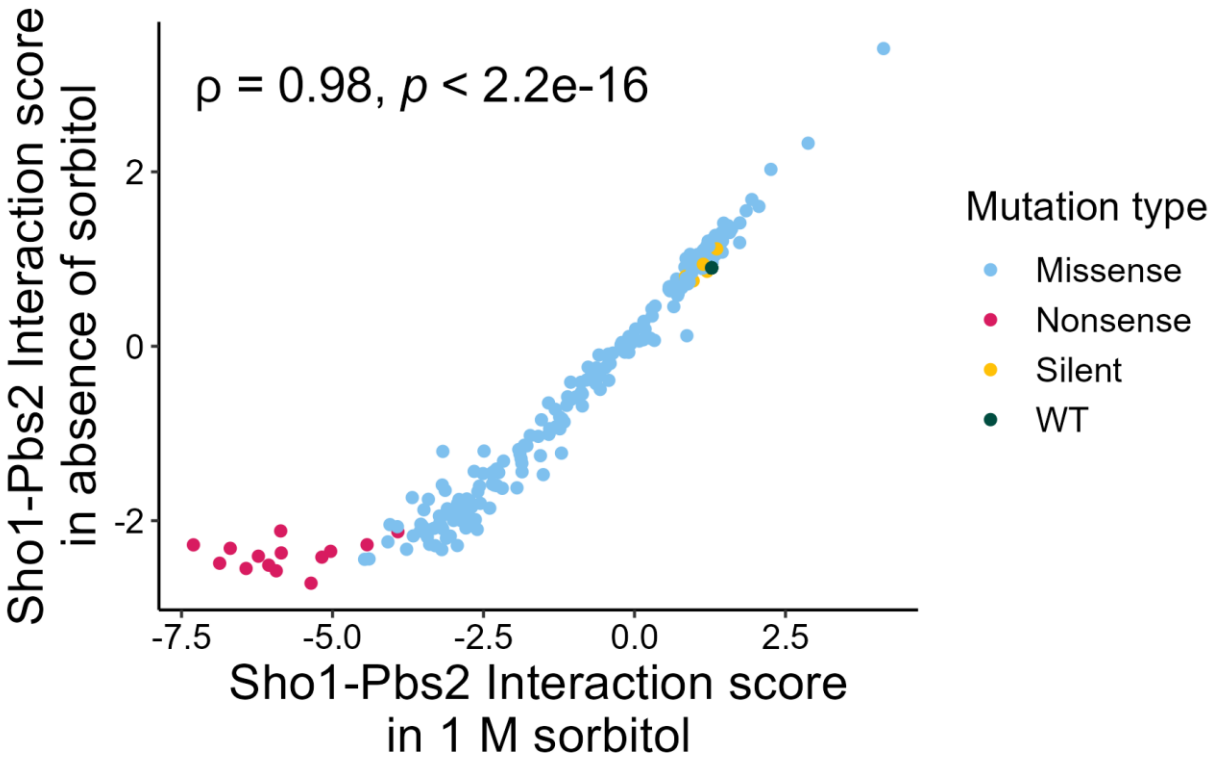

Figure S7.

Scatterplot of the Sho1 interaction scores for all mutants in the Pbs2 extended motif DMS library, in the presence and absence of 1 M of sorbitol. Measurements in DHFR-PCA media with methotrexate. The correlation has a spearman's rho 0.98, and a p-value < $2.2X10^{-16}$. The measurements for the interaction in 1 M sorbitol have a greater range due to the greater activation of the HOG pathway.

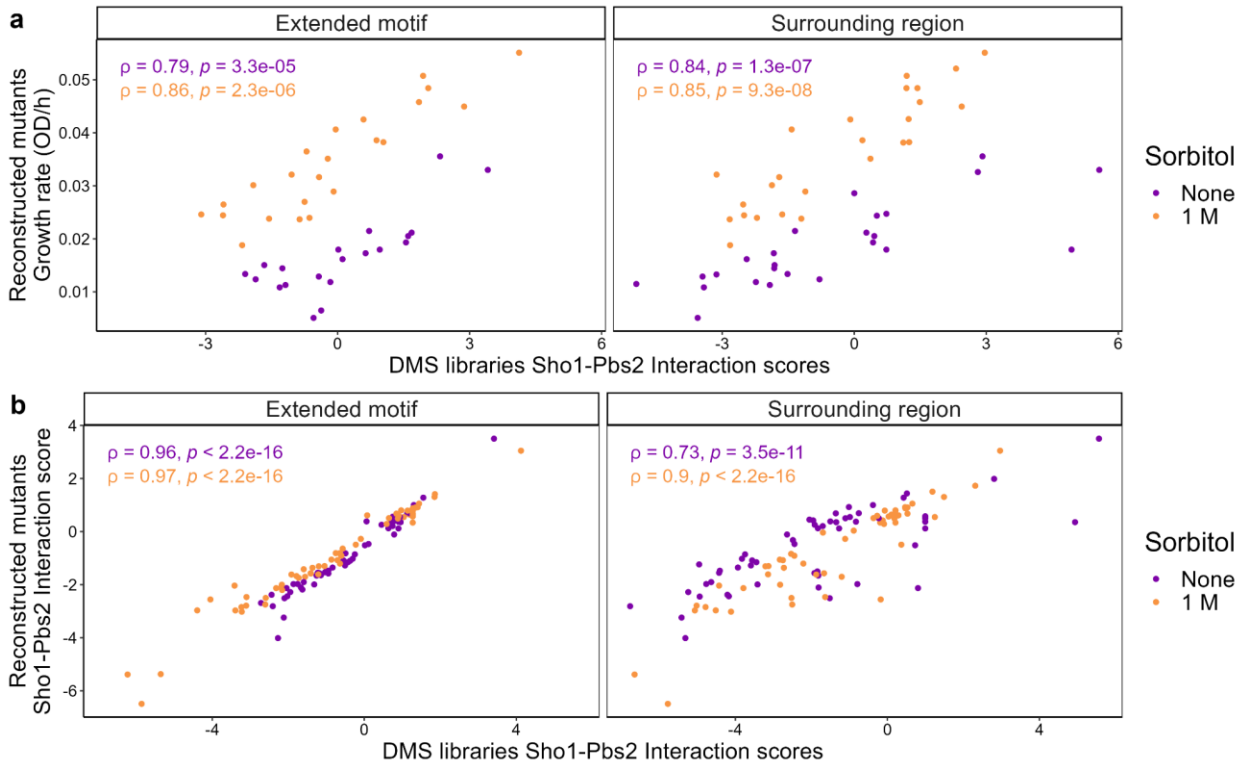

Figure S8.

Validation of pooled DHFR-PCA effects by individually reconstructed mutants

a) Scatterplot of Sho1-Pbs2 interaction scores as measured in pooled competition DHFR-PCA of the DMS libraries (x-axis) and growth rate of the same mutations individually reconstructed, in DHFR-PCA growth curves (y-axis). Results from the DMS library of the surrounding region (left) and the DMS library of the extended motif (right), in the presence (orange) or absence (purple) of 1 M of sorbitol. The spearman correlations between the two methods of measuring the interaction strength are indicated on the plots.

b) Scatterplot of Sho1-Pbs2 interaction scores as measured in pooled competition DHFR-PCA of the DMS libraries (x-axis) and measured in pooled competition DHFR-PCA of individually reconstructed mutants (y-axis). Results from the DMS library of the surrounding region (left) and the DMS library of the extended motif (right), in the presence (orange) or absence (purple) of 1 M of sorbitol. The spearman correlations between the two methods of measuring the interaction strength are indicated on the plots.

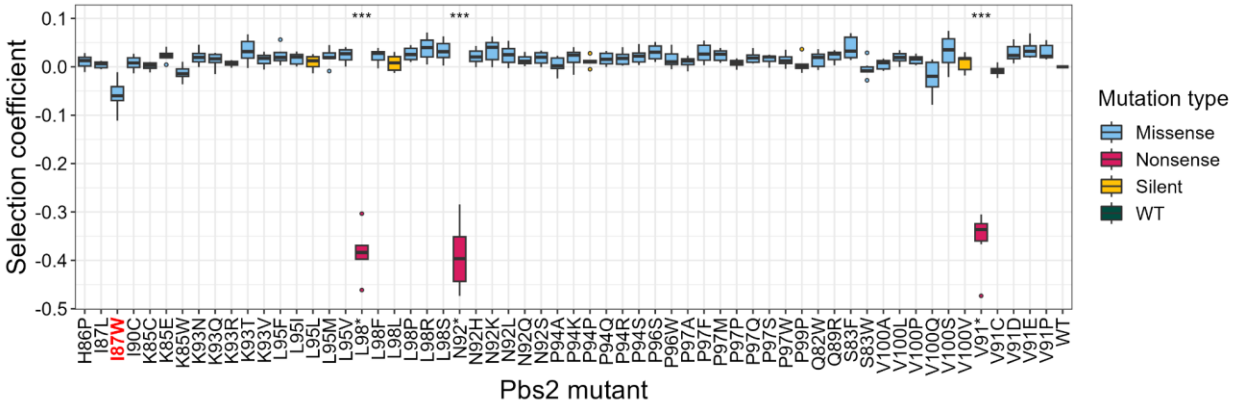

Figure S9.

Impact on growth rate measured as selection coefficients for individually reconstructed Pbs2 mutants in SC synthetic media with 1 M sorbitol. The strains contain no DHFR fragments on any proteins. Boxplots show the distribution of 6 replicates per mutant. The selection coefficient is normalized by the growth of the wild-type sequence, making the wild-type selection coefficient zero. Only the 3 nonsense mutants grew significantly less than wild-type Pbs2 and the silent mutants (Welch's t-test with false discovery rate correction p-value < 0.05), although I87W (highlighted in red on axis), which is the mutant with the highest Sho1-Pbs2 interaction score shows a marked decrease in selection coefficient (p-value = 0.066).

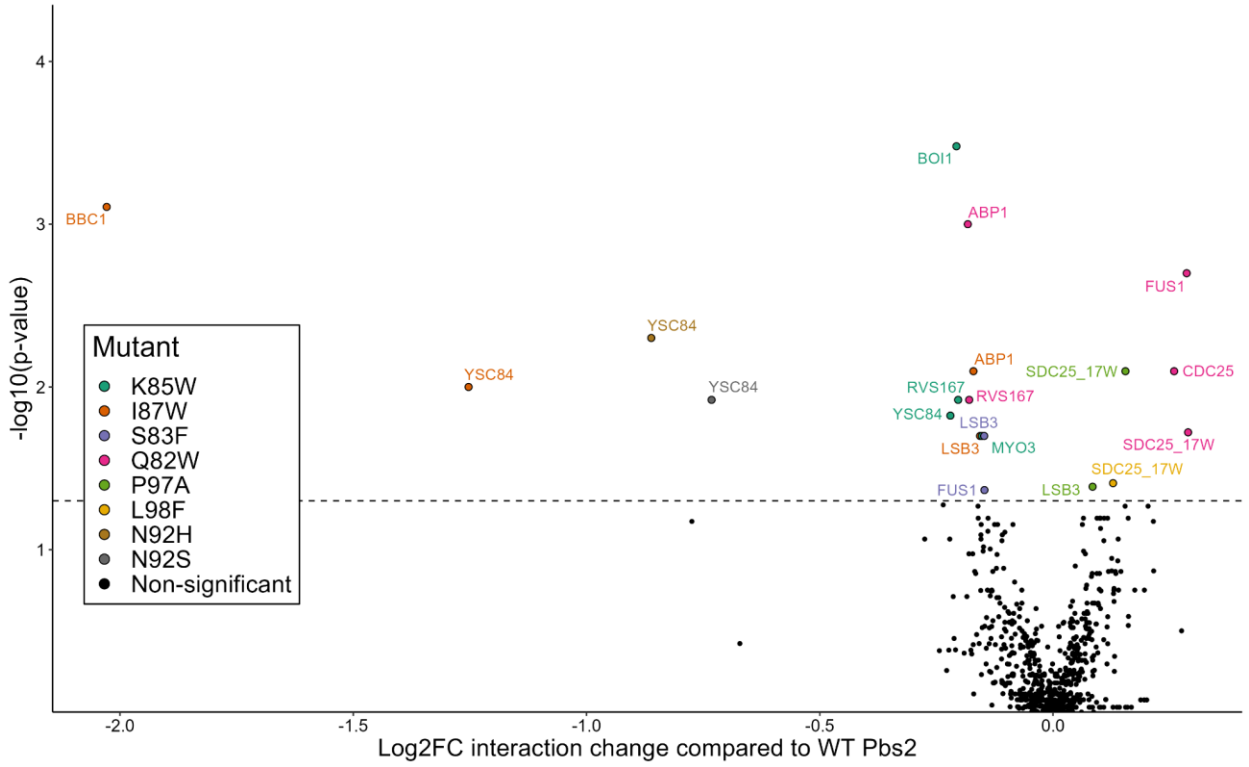

Figure S10.

Volcano plot comparing the binding of Pbs2 mutants to SH3 domain containing proteins and wild-type Pbs2 binding to the same SH3 domain containing proteins. Each dot represents one Pbs2 mutant interaction with one of the 23 SH3 containing proteins present in yeast, not considering Nbp2. On the x-axis, the interaction strength of the mutant Pbs2 with a certain SH3 containing protein is compared to the interaction strength of wild-type Pbs2 with the same SH3 containing protein by calculating the log2-fold change between the two interaction scores. A positive value therefore indicates a loss of specificity (stronger binding by the mutant than by the wild type) and a negative value indicates a gain of specificity (weaker binding by the mutant than by the wild type). On the y-axis, the negative log10 transformation of the p-value (two-sided Welch's t-test with false discovery rate correction), of the same comparison is shown. The interactions with a false discovery rate corrected p-value below 0.05 are coloured by the Pbs2 mutant and the SH3 containing protein is labeled. The dashed line indicates the p-value cut-off of 0.05.

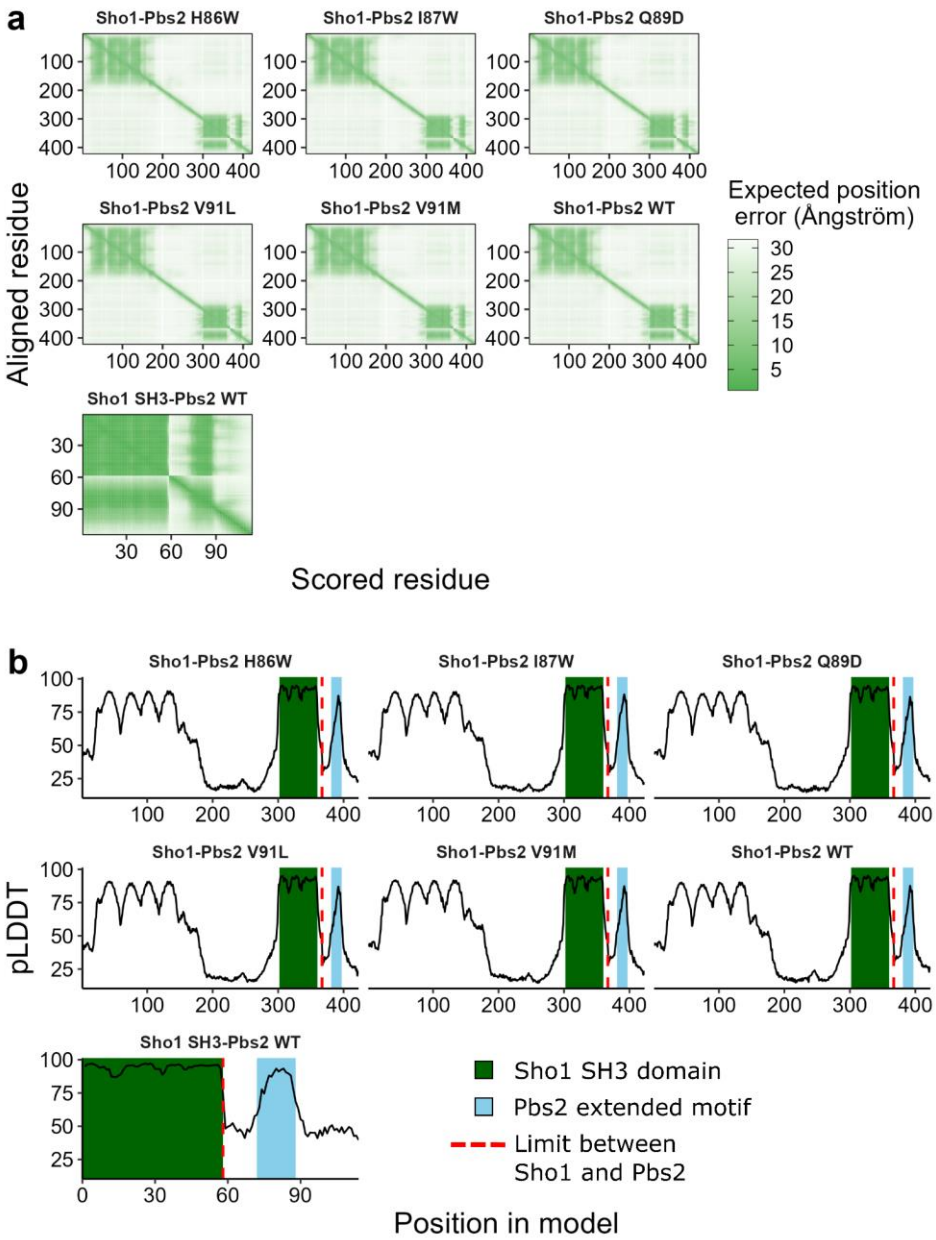

Figure S11.

Confidence metrics for the seven structures predicted using AlphaFold2-Multimer. Sho1 SH3-Pbs2 WT is the structure in figure 2b, Sho1-Pbs2 WT is the structure in figure 4a, Sho1-Pbs2 I87W is the structure in figure 4b, and all others are the structures with the same Pbs2 mutants in figure S12. a) Predicted aligned error (PAE) values for the 7 predicted structures, output from AlphaFold-Multimer. b) pLDDT value for each position in the 7 predicted structures, output from AlphaFold-Multimer. Positions corresponding to the SH3 domain of Sho1 are indicated by a green background, and positions corresponding to the extended motif of Pbs2 are indicated by a blue background. Since AlphaFold-Multimer combines the sequences of both proteins into a single model, a red dashed line was used to mark the end of the Sho1 portion of the model, and the beginning of the Pbs2 portion of the model.

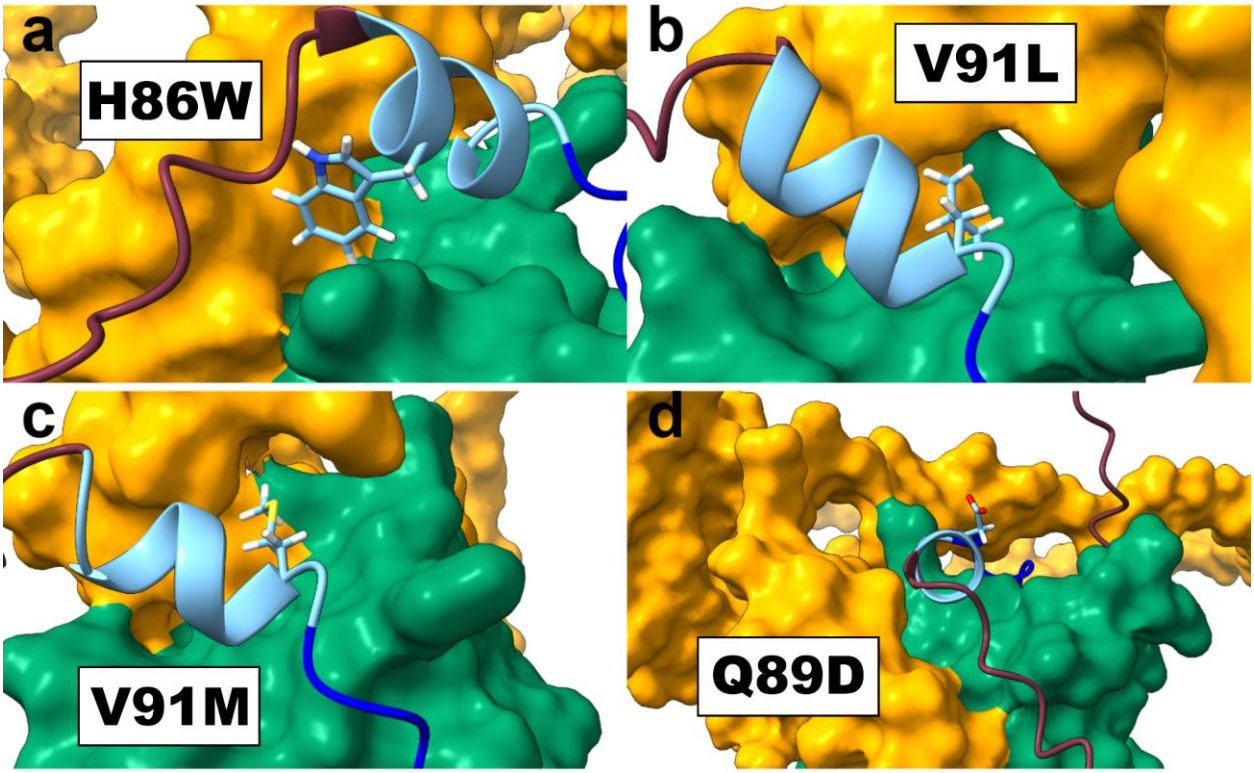

Figure S12.
Close-up details of AlphaFold-Multimer predicted complexes of Sho1 with Pbs2 mutants a) H86W, b) V91L, c) V91M and d) Q89D. The predicted structures are colored as in panel a of figure 4, with the SH3 domain of Sho1 in green, the non-SH3 portions of Sho1 in orange, the core motif of Pbs2 in dark blue, the extended motif (apart from the core motif) in light blue and the flanking sequences in burgundy. The side chain of the mutated residue is shown with oxygen atoms in red, nitrogen atoms in blue, sulfur atoms in yellow, hydrogen atoms in white and carbon atoms the same color as the extended motif, while all other side chains in Pbs2 are hidden.

Literature cited

Amberg D., D. C. Burke, and J. N. Strathern, 2005 *Methods in yeast genetics: a Cold Spring Harbor Laboratory course manual*. Cold Spring Harbor Laboratory Press, Cold Spring Harbor, N.Y.

Andrews S., 2010 FastQC: a quality control tool for high throughput sequence data

Attali D., and C. Baker, 2023 *ggExtra: Add Marginal Histograms to "ggplot2", and More "ggplot2" Enhancements*.

Bendel A. M., A. J. Faure, D. Klein, K. Shimada, G. Kempf, *et al.*, 2023 The genetic architecture of protein interaction affinity and specificity. bioRxiv 2023.10.17.562688.

Bolger A. M., M. Lohse, and B. Usadel, 2014 Trimmomatic: a flexible trimmer for Illumina sequence data. Bioinformatics 30: 2114–2120.

Dalgarno D. C., M. C. Botfield, and R. J. Rickles, 1997 SH3 domains and drug design: Ligands, structure, and biological function. Pept. Sci. 43: 383–400.

Després P. C., A. F. Cisneros, E. M. M. Alexander, R. Sonigara, C. Gagné-Thivierge, *et al.*, 2022 Asymmetrical dose responses shape the evolutionary trade-off between antifungal resistance and nutrient use. Nat Ecol Evol 6: 1501–1515.

Dibyachintan S., A. K. Dube, D. Bradley, P. Lemieux, U. Dionne, *et al.*, 2024 Cryptic genetic variation shapes the fate of gene duplicates in a protein interaction network. bioRxiv 2024.02.23.581840.

Dionne U., É. Bourgault, A. K. Dubé, D. Bradley, F. J. M. Chartier, *et al.*, 2021 Protein context shapes the specificity of SH3 domain-mediated interactions in vivo. Nat. Commun. 12: 1597.

Dionne U., L. J. Percival, F. J. M. Chartier, C. R. Landry, and N. Bisson, 2022 SRC homology 3 domains: multifaceted binding modules. Trends Biochem. Sci. 47: 772–784.

Diss G., and B. Lehner, 2018 The genetic landscape of a physical interaction. Elife 7. https://doi.org/10.7554/eLife.32472

Dubé A. K., R. Dandage, S. Dibyachintan, U. Dionne, P. C. Després, *et al.*, 2022 Deep Mutational Scanning of Protein–Protein Interactions Between Partners Expressed from Their Endogenous Loci In Vivo, pp. 237–259 in *Yeast Functional Genomics: Methods and Protocols*, edited by Devaux F. Springer US, New York, NY.

Ernst A., D. Gfeller, Z. Kan, S. Seshagiri, P. M. Kim, *et al.*, 2010 Coevolution of PDZ domain-ligand interactions analyzed by high-throughput phage display and deep sequencing. Mol. Biosyst. 6: 1782–1790.

Evans R., M. O'Neill, A. Pritzel, N. Antropova, A. Senior, *et al.*, 2022 Protein complex prediction with AlphaFold-Multimer. bioRxiv 2021.10.04.463034.

Faure A. J., J. Domingo, J. M. Schmiedel, C. Hidalgo-Carcedo, G. Diss, *et al.*, 2022 Mapping the energetic and allosteric landscapes of protein binding domains. Nature 604: 175–183.

Feng S., C. Kasahara, R. J. Rickles, and S. L. Schreiber, 1995 Specific interactions outside the proline-rich core of two classes of Src homology 3 ligands. Proc. Natl. Acad. Sci. U. S. A. 92: 12408–12415.

Ferrigno P., F. Posas, D. Koepp, H. Saito, and P. A. Silver, 1998 Regulated nucleo/cytoplasmic exchange of HOG1 MAPK requires the importin beta homologs NMD5 and XPO1. EMBO J. 17: 5606–5614.

Fowler D. M., and S. Fields, 2014 Deep mutational scanning: a new style of protein science. Nat. Methods 11: 801–807.

Freschi L., F. Torres-Quiroz, A. K. Dubé, and C. R. Landry, 2013 qPCA: a scalable assay to measure the perturbation of protein-protein interactions in living cells. Mol. Biosyst. 9: 36–43.

Gaussmann S., R. Peschel, J. Ott, K. M. Zak, J. Sastre, *et al.*, 2024 Modulation of peroxisomal import by the PEX13 SH3 domain and a proximal FxxxF binding motif. Nat. Commun. 15: 3317.

Gouw M., S. Michael, H. Sámano-Sánchez, M. Kumar, A. Zeke, *et al.*, 2018 The eukaryotic linear motif resource – 2018 update. Nucleic Acids Res. 46: D428–D434.

Gueldener U., J. Heinisch, G. J. Koehler, D. Voss, and J. H. Hegemann, 2002 A second set of loxP marker cassettes for Cre-mediated multiple gene knockouts in budding yeast. Nucleic Acids Res. 30: e23.

Harris C. R., K. J. Millman, S. J. van der Walt, R. Gommers, P. Virtanen, *et al.*, 2020 Array programming with NumPy. Nature 585: 357–362.

Haslam N. J., and D. C. Shields, 2012 Peptide-Binding Domains: Are Limp Handshakes Safest? Sci. Signal. 5: e40–pe40.

Hunter J. D., 2007 Matplotlib: A 2D Graphics Environment. Comput. Sci. Eng. 9: 90–95.

Illumina, Nextera DNA Indexes. Illumina Support Docs.

ImageMagick Studio LLC, 2023 *ImageMagick*.

Ivarsson Y., and P. Jemth, 2019 Affinity and specificity of motif-based protein-protein interactions. Curr. Opin. Struct. Biol. 54: 26–33.

Jumper J., R. Evans, A. Pritzel, T. Green, M. Figurnov, *et al.*, 2021 Highly accurate protein structure prediction with AlphaFold. Nature 596: 583–589.

Kamrad S., M. Rodríguez-López, C. Cotobal, C. Correia-Melo, M. Ralser, *et al.*, 2020 Pyphe, a python toolbox for assessing microbial growth and cell viability in high-throughput colony

screens. Elife 9. https://doi.org/10.7554/eLife.55160

Kaneko T., L. Li, and S. S.-C. Li, 2008 The SH3 domain--a family of versatile peptide- and protein-recognition module. Front. Biosci. 13: 4938–4952.

Kaneko T., H. Huang, X. Cao, X. Li, C. Li, *et al.*, 2012 Superbinder SH2 Domains Act as Antagonists of Cell Signaling. Sci. Signal. 5: ra68–ra68.

Karlsson O. A., G. N. Sundell, E. Andersson, Y. Ivarsson, and P. Jemth, 2016 Improved affinity at the cost of decreased specificity: a recurring theme in PDZ-peptide interactions. Sci. Rep. 6: 34269.

Kassambara A., 2020 ggpubr: “ggplot2” Based Publication Ready Plots

Kassambara A., 2021 rstatix: Pipe-Friendly Framework for Basic Statistical Tests

Kazlauskas A., C. Schmotz, T. Kesti, J. Hepojoki, I. Kleino, *et al.*, 2016 Large-Scale Screening of Preferred Interactions of Human Src Homology-3 (SH3) Domains Using Native Target Proteins as Affinity Ligands. Mol. Cell. Proteomics 15: 3270–3281.

Keck F., 2020 Handling biological sequences in R with the bioseq package. Methods Ecol. Evol. 11: 1728–1732.

Kelil A., E. D. Levy, and S. W. Michnick, 2016 Evolution of domain–peptide interactions to coadapt specificity and affinity to functional diversity. Proc. Natl. Acad. Sci. U. S. A. 113: E3862–E3871.

Kelil A., B. Dubreuil, E. D. Levy, and S. W. Michnick, 2017 Exhaustive search of linear information encoding protein-peptide recognition. PLoS Comput. Biol. 13: e1005499.

Kijima Y., D. Evans-Yamamoto, H. Toyoshima, and N. Yachie, 2023 A universal sequencing

read interpreter. Sci Adv 9: eadd2793.

Kursula P., I. Kursula, Y. H. Song, K. Paraskevopoulos, and M. Wilmanns, 2008 YEAST SHO1 SH3 DOMAIN COMPLEXED WITH A PEPTIDE FROM PBS2

Langmead B., C. Trapnell, M. Pop, and S. L. Salzberg, 2009 Ultrafast and memory-efficient alignment of short DNA sequences to the human genome. Genome Biol. 10: R25.

Lee C. H., K. Saksela, U. A. Mirza, B. T. Chait, and J. Kuriyan, 1996 Crystal structure of the conserved core of HIV-1 Nef complexed with a Src family SH3 domain. Cell 85: 931–942.

Lemieux P., D. Bradley, A. K. Dubé, U. Dionne, and C. R. Landry, 2024 Dissection of the role of a Src homology 3 domain in the evolution of binding preference of paralogous proteins. Genetics 226. https://doi.org/10.1093/genetics/iyad175

Li S. S.-C., 2005 Specificity and versatility of SH3 and other proline-recognition domains: structural basis and implications for cellular signal transduction. Biochem. J 390: 641–653.

Maeda T., M. Takekawa, and H. Saito, 1995 Activation of Yeast PBS2 MAPKK by MAPKKKs or by Binding of an SH3-Containing Osmosensor. Science 269: 554–558.

Mapes J., and I. M. Ota, 2004 Nbp2 targets the Ptc1-type 2C Ser/Thr phosphatase to the HOG MAPK pathway. EMBO J. 23: 302–311.

Marles J. A., S. Dahesh, J. Haynes, B. J. Andrews, and A. R. Davidson, 2004 Protein-Protein Interaction Affinity Plays a Crucial Role in Controlling the Sho1p-Mediated Signal Transduction Pathway in Yeast. Mol. Cell 14: 813–823.

Martin M., 2011 Cutadapt removes adapter sequences from high-throughput sequencing reads. EMBnet.journal 17: 10–12.

Masella A. P., A. K. Bartram, J. M. Truszkowski, D. G. Brown, and J. D. Neufeld, 2012 PANDAseq: paired-end assembler for illumina sequences. BMC Bioinformatics 13: 31.

Messing J., 1983 [2] New M13 vectors for cloning, pp. 20–78 in *Methods in Enzymology*, Academic Press.

Michnick S. W., E. D. Levy, C. R. Landry, J. Kowarzyk, and V. Messier, 2016 The Dihydrofolate Reductase Protein-Fragment Complementation Assay: A Survival-Selection Assay for Large-Scale Analysis of Protein–Protein Interactions. Cold Spring Harb. Protoc. 2016: db.prot090027.

Miyazaki K., 2011 Chapter seventeen - MEGAWHOP Cloning: A Method of Creating Random Mutagenesis Libraries via Megaprimer PCR of Whole Plasmids, pp. 399–406 in *Methods in Enzymology*, Synthetic Biology, Part B. edited by Voigt C. Academic Press.

Monera O. D., T. J. Sereda, N. E. Zhou, C. M. Kay, and R. S. Hodges, 1995 Relationship of sidechain hydrophobicity and alpha-helical propensity on the stability of the single-stranded amphipathic alpha-helix. J. Pept. Sci. 1: 319–329.

Murakami Y., K. Tatebayashi, and H. Saito, 2008 Two adjacent docking sites in the yeast Hog1 mitogen-activated protein (MAP) kinase differentially interact with the Pbs2 MAP kinase kinase and the Ptp2 protein tyrosine phosphatase. Mol. Cell. Biol. 28: 2481–2494.

Pawson T., M. Raina, and P. Nash, 2002 Interaction domains: from simple binding events to complex cellular behavior. FEBS Lett. 513: 2–10.

Pettersen E. F., T. D. Goddard, C. C. Huang, E. C. Meng, G. S. Couch, *et al.*, 2021 UCSF ChimeraX: Structure visualization for researchers, educators, and developers. Protein Sci. 30: 70–82.

Posas F., and H. Saito, 1997 Osmotic Activation of the HOG MAPK Pathway via Ste11p MAPKKK: Scaffold Role of Pbs2p MAPKK. Science 276: 1702–1705.

R Core Team, 2023 *R: A Language and Environment for Statistical Computing*. R Foundation for Statistical Computing, Vienna, Austria.

Rice P., I. Longden, and A. Bleasby, 2000 EMBOSS: the European Molecular Biology Open Software Suite. Trends Genet. 16: 276–277.

Rickles R. J., M. C. Botfield, X. M. Zhou, P. A. Henry, J. S. Brugge, *et al.*, 1995 Phage display selection of ligand residues important for Src homology 3 domain binding specificity. Proc. Natl. Acad. Sci. U. S. A. 92: 10909–10913.

Robles J. T., H. J. Lou, G. Shi, P. L. Pan, and B. E. Turk, 2023 Linear motif specificity in signaling through p38α and ERK2 mitogen–activated protein kinases. Proceedings of the National Academy of Sciences 120: e2316599120.

Rochette S., G. Diss, M. Filteau, J.-B. Leducq, A. K. Dubé, *et al.*, 2015 Genome-wide protein-protein interaction screening by protein-fragment complementation assay (PCA) in living cells. J. Vis. Exp. https://doi.org/10.3791/52255

Rognes T., T. Flouri, B. Nichols, C. Quince, and F. Mahé, 2016 VSEARCH: a versatile open source tool for metagenomics. PeerJ 4: e2584.

Ryan O. W., S. Poddar, and J. H. D. Cate, 2016 CRISPR-Cas9 Genome Engineering in Saccharomyces cerevisiae Cells. Cold Spring Harb. Protoc. 2016. https://doi.org/10.1101/pdb.prot086827

Saito H., and F. Posas, 2012 Response to Hyperosmotic Stress. Genetics 192: 289–318.

Schloerke B., D. Cook, J. Larmarange, F. Briatte, M. Marbach, *et al.*, 2023 *GGally: Extension to*

"ggplot2."

Slowikowski K., 2023 *ggrepel: Automatically Position Non-Overlapping Text Labels with "ggplot2."*

Stein A., and P. Aloy, 2008 Contextual specificity in peptide-mediated protein interactions. PLoS One 3: e2524.

Tarassov K., V. Messier, C. R. Landry, S. Radinovic, M. M. S. Molina, *et al.*, 2008 An in Vivo Map of the Yeast Protein Interactome. Science 320: 1465–1470.

Tatebayashi K., K. Yamamoto, K. Tanaka, T. Tomida, T. Maruoka, *et al.*, 2006 Adaptor functions of Cdc42, Ste50, and Sho1 in the yeast osmoregulatory HOG MAPK pathway. EMBO J. 25: 3033–3044.

The pandas development team, 2023 *pandas-dev/pandas: Pandas*.

Tonikian R., X. Xin, C. P. Toret, D. Gfeller, C. Landgraf, *et al.*, 2009 Bayesian Modeling of the Yeast SH3 Domain Interactome Predicts Spatiotemporal Dynamics of Endocytosis Proteins. PLoS Biol. 7: e1000218.

Van Roey K., B. Uyar, R. J. Weatheritt, H. Dinkel, M. Seiler, *et al.*, 2014 Short Linear Motifs: Ubiquitous and Functionally Diverse Protein Interaction Modules Directing Cell Regulation. Chem. Rev. 114: 6733–6778.

Vincentelli R., K. Luck, J. Poirson, J. Polanowska, J. Abdat, *et al.*, 2015 Quantifying domain-ligand affinities and specificities by high-throughput holdup assay. Nat. Methods 12: 787–793.

Wang C.-H., P. Mehta, and C. J. Bashor, 2018 The strength of protein-protein interactions controls the information capacity and dynamical response of signaling networks. bioRxiv

469197.

Wickham H., M. Averick, J. Bryan, W. Chang, L. D. McGowan, *et al.*, 2019 Welcome to the tidyverse. Journal of Open Source Software 4: 1686.

Wilke C. O., 2020 cowplot: Streamlined Plot Theme and Plot Annotations for “ggplot2”

Zarin T., and B. Lehner, 2024 A complete map of specificity encoding for a partially fuzzy protein interaction. bioRxiv 2024.04.25.591103.

Zarrinpar A., S.-H. Park, and W. A. Lim, 2003 Optimization of specificity in a cellular protein interaction network by negative selection. Nature 426: 676–680.

Zarrinpar A., R. P. Bhattacharyya, M. P. Nittler, and W. A. Lim, 2004 Sho1 and Pbs2 Act as Coscaffolds Linking Components in the Yeast High Osmolarity MAP Kinase Pathway. Mol. Cell 14: 825–832.